Review of the influence of the interaction between in-plane and out-of-plane behaviors on the seismic response of framed unreinforced masonry walls

Ghezelbash, Amirhossein; Rots, Jan G.; Messali, Francesco

DOI
10.1016/j.istruc.2025.110271

Publication date
2025

Document Version
Final published version

Published in
Structures

Structures 81 (2025) 110271

Contents lists available at ScienceDirect

Structures

journal homepage: www.elsevier.com/locate/structures

Review of the influence of the interaction between in-plane and out-of-plane behaviors on the seismic response of framed unreinforced masonry walls

Amirhossein Ghezelbash *, Jan G. Rots, Francesco Messali

Faculty of Civil Engineering and Geosciences – Delft University of Technology, Delft, the Netherlands

ARTICLE INFO

Keywords:
Unreinforced masonry
Interaction
In-plane
Out-of-plane
Seismic response
Framed walls

ABSTRACT

This paper presents a comprehensive review of the effects of interactions between in-plane (IP) and out-of-plane (OOP) behaviors, referred to as IP-OOP interactions, on the seismic behavior of framed unreinforced masonry structures, consolidating findings from experimental, numerical, and analytical studies available in the literature. While masonry structures are highly vulnerable to seismic loading and undergo multi-directional seismic actions, most existing research focuses on their response to unidirectional forces, overlooking the complex interaction effects observed during real earthquakes. Moreover, although design and assessment standards acknowledge these interactions, they offer limited prescriptive guidance. The literature predominantly addresses the impact of IP pre-damage on OOP strength and stability (IP/OOP interaction), with comparatively fewer studies examining the reverse scenario, i.e., OOP pre-loading affecting IP resistance (OOP/IP interaction). Experimental data remains scarce, particularly for multi-bay frames and walls with openings, limiting the generalizability of current findings. Numerical simulations have significantly advanced the understanding of these interactions, yet their reliability relies on proper calibration against benchmark experiments, which are still limited in number. Among the most influential parameters affecting the effect of IP pre-damage on the OOP response, the height-to-thickness slenderness ratio plays a dominant role. Slender walls are especially prone to severe OOP strength degradation due to reduced arching action and increased instability. The length-to-height aspect ratio also influences failure modes under IP/OOP interaction, particularly in short walls where horizontal arching action reduces. Other critical factors, such as masonry material properties, boundary conditions, and frame stiffness, have been identified, but their effects remain less systematically studied. Analytical approaches have primarily focused on IP/OOP interaction effects. However, existing equations are often derived from limited datasets, restricting their predictive capabilities. The equation widely adopted in seismic guidelines has been shown to overestimate OOP strength reduction, underscoring the need for more refined models that incorporate broader experimental and numerical data. Future research should address these gaps by expanding experimental campaigns, enhancing numerical methodologies, and refining analytical frameworks to better represent real-world conditions.

1. Introduction

Framed masonry structures are widely used in both residential and commercial construction due to their cost-effectiveness, ease of construction, and satisfactory structural performance under gravity loading [1]. In these structures, unreinforced (URM) masonry walls act as panels infilled or confined within reinforced concrete or steel frames, providing partitioning and contributing to thermal and acoustic insulation [2,3]. One of the primary concerns in seismic design is the vulnerability of framed masonry structures to earthquake-induced damage [4]. While traditionally considered non-structural elements, the URM walls within frames can significantly influence the overall behavior of the frame under lateral loads [5]. Their presence can enhance stiffness and strength, altering the dynamic response of the structure [6]. However, framed walls also introduce complexities in load distribution and failure mechanisms, particularly under seismic actions [7]. Framed walls can experience brittle failures, leading to the formation of diagonal cracks, crushing, or out-of-plane collapse [8]. In many cases, severe damage to framed walls can compromise the lateral stability of the entire structure,

* Corresponding author.
E-mail address: a.ghezelbash@tudelft.nl (A. Ghezelbash).

https://doi.org/10.1016/j.istruc.2025.110271
Received 14 July 2025; Received in revised form 28 August 2025; Accepted 19 September 2025
Available online 2 October 2025

Nomenclature

Abbreviation (General Terms)

IP	In-Plane
OOP	Out-of-Plane
URM	Unreinforced Masonry

Interaction Scenarios

IP-OOP	Influence of IP response on OOP behavior of walls and vice versa
IP/OOP	Effects of IP pre-damage, pre-deformation, pre-load, or concurrent load on OOP response of walls
OOP/IP	Effects of OOP pre-damage, pre-deformation, pre-load, or concurrent load on IP response of walls

Numerical Modeling Approaches

CoB	Continuum-Based
ME	Macro-Element
SMSBB	Simplified Micro-Scale Block-Based

Specimen Type

CM	Confined Masonry
IM	Infilled Masonry

Masonry Unit Type

HCB	Hollow Concrete Block/Brick
HCLB	Hollow Clay Block/Brick
SCB	Solid Concrete Brick
SCLB	Solid Clay Brick

Masonry Unit Configuration

f'_m	Masonry Prism Compressive Strength
H	Horizontal Holes
V	Vertical Holes

Mortar Type and Configuration

C	Cement
DHJ	Dry Head Joints
L	Lime
S	Sand

Frame Type

RC	Reinforced Concrete

Opening Type and Position

D	Door
PF	Partially Filled
W	Window

Wall/Frame Configuration

Ba	Bay
Cav	Cavity Wall
Q	Quadruple-Bay
St	Story

Geometrical Properties

h/t	Height/Thickness Slenderness Ratio
l/h	Length/Height Aspect Ratio
t	Panel Thickness

Loading Scenarios

SQ	Sequential
SC	Successive
CB	Combined
SM	Simultaneous

Loading Sequences

IP, OOP	IP load, then OOP
IP, OOP, IP	Alternative loading starting from IP
IP + OOP	Concurrent IP and OOP loads
OOP, IP	OOP load, then IP
OOP, IP, OOP	Alternative loading starting from OOP

Loading Procedures

Dyn	Dynamic
QSC	Quasi-Static Cyclic
QSLUC	Quasi-Static Load-Unload Cycles
QSM	Quasi-Static Monotonic

Loading Apparatus

AB	Airbag (Wall Face Pressure)
FD	Frame Displacement
AV	Ambient Vibration
ST	Shake Table
WF4PL	Wall Face Four-Point Load
WF5PL	Wall Face Five-Point Load
WF6PL	Wall Face Six-Point Load
WFMiPL	Wall Face Middle-Point Load

Boundary Conditions

1WB	One-Way Bending
2WB	Two-Way Bending
B	Beam-like
Ct	Cantilever
DC	Double-Clamped

increasing the risk of partial or total collapse [9]. Understanding the seismic behavior of framed masonry systems is therefore critical for improving their resilience [10].

While many experimental and numerical investigations have focused on either in-plane (IP) or out-of-plane (OOP) behavior separately, real-world earthquakes impose multi-directional forces, creating complex interactions between the two response modes [11,12]. Several studies have highlighted that damage induced by IP deformation can reduce the OOP capacity of masonry walls, leading to premature failure [3,13–15]. Conversely, OOP deformation can alter the stiffness and strength characteristics of framed walls, influencing their in-plane resistance [16]. Despite these findings, research explicitly considering IP and OOP interaction effects remains limited. Most available studies simplify the problem by investigating masonry responses under isolated unidirectional loading conditions, neglecting the impact of concurrent multi-directional seismic demands [17]. This knowledge gap poses challenges in accurately predicting failure mechanisms and designing reliable mitigation strategies.

This paper aims to provide a comprehensive review of the literature on IP and OOP interaction effects in framed unreinforced masonry structures. It consolidates findings from experimental, numerical, and analytical studies to assess the current state of knowledge and identify key gaps that require further investigation. Particular emphasis is placed on identifying influential parameters governing the interaction effects in the response of the walls, evaluating the limitations of existing design methodologies, and discussing the applicability of analytical and macro-element modeling approaches for large-scale structural assessments. In addition to synthesizing existing research, this paper introduces a novel, consistent terminology for describing IP and OOP interaction effects, addressing the current lack of standardization in the field and enabling clearer communication and comparison across studies. The paper is structured as follows. First, a clear definition of the IP and OOP

interaction effects considered within the scope of this study is provided in 2. Then, the landscape of the current experimental and numerical works published on the study of IP and OOP interaction effects in framed URM walls is provided in 3, followed by the detailed review of these studies to identify the extent of interaction effects at wall level as well as parameters most influencing it or not studied enough in 4. In 5, an assessment is presented for existing analytical formulations and macro-element models developed based on wall-level studies for the estimation of building-level responses under interaction effects. The knowledge gaps identified during the review are summarized in 6. Finally, concluding remarks identifying research gaps and future directions for improving seismic design and assessment practices are discussed in 7. It should be noted that a similar review is conducted for IP and OOP interaction effects in non-framed URM walls, i.e., regular walls not enclosed within a surrounding frame. However, due to the fundamental differences in the manifestation of interaction effects between framed and non-framed configurations, it is omitted here to maintain conciseness. Interested readers are referred to [18] for further details.

2. Definition of "in-plane and out-of-plane interaction effects" in framed URM walls

Despite the considerable number of experimental and numerical studies on the interaction between IP and OOP behaviors in framed URM walls, a unified definition of these interactions and the scenarios in which they occur does not exist in the literature. As a result, various non-interchangeable terminologies have emerged in the literature, often describing fundamentally different interaction scenarios. To address this gap, the present study proposes a structured classification system that consistently defines and categorizes the different types and scenarios of interaction using a set of uniform terminologies that encompass all possible variations. In the manuscript, the term "IP-OOP interaction effects" in a framed URM wall refers to any influence that IP loading, deformation, or damage of the wall has on its OOP behavior, referred to as "IP/OOP interaction," and any influence that OOP loading, deformation, or damage of the wall has on its IP behavior, referred to as "OOP/IP interaction." Since framed walls are considered isolated elements behaving individually rather than together with the panels of adjacent bays or stories, the other type of interaction wherein the IP and OOP responses of walls within a structure can, respectively, influence the OOP and IP behaviors of perpendicular walls intersecting with it, and vice versa, is neglected.

Either of the IP/OOP and OOP/IP interaction types can appear and be studied under different scenarios identified in the literature, which include the sequential (SQ), successive (SC), combined (CB), or simultaneous (SM) application of IP and OOP loads, as shown in Fig. 1. In SQ loading, the wall is loaded and unloaded once in one of the IP or OOP lateral directions, and then the load is applied in the other orthogonal direction. Also, in the case of SC loading, the IP and OOP loads are applied separately. However, unlike SQ, multiple sequences of IP and OOP loadings are applied in succession to represent the effects of repeated loading and damage histories. In the case of CB loading, the tests are conducted by first applying an IP or OOP pre-load or pre-deformation in one lateral direction. Afterwards, the pre-load or pre-deformation is maintained constant, while the wall is loaded in the orthogonal direction. It is important to note that when a load is pre-applied, its resultant deformation can change during the subsequent loading step. On the other hand, when pre-deformation is applied, the force causing it can change during the subsequent steps, and hence, resulting in a different behavior than that obtained from the application of a pre-load. In the case of SM loading, the IP and OOP loads or deformations are applied simultaneously with different levels of intensity for each of the orthogonal directions. The different loading sequences used for each interaction scenario are further distinguished via the terminology shown in Fig. 1. Specifically, the term "IP, OOP" is used for loading sequences that start with IP pre-damage or pre-deformation in the SQ or CB scenarios, and "IP, OOP, IP" is used for a similar sequence in the SC scenario. The term "OOP, IP" denotes SQ or CB loadings starting in the OOP direction, and "OOP, IP, OOP" is used for a similar sequence in the SC scenario. Finally, the simultaneous application of IP and OOP loads and deformation in the SM scenario is indicated with "IP + OOP."

The loading scenarios adopted in the study of IP-OOP interaction effects can be used to simulate pre-loads, pre-damage, and pre-deformations arising from a range of real-world sources. Some structures may have experienced foundation settlement or rotation, resulting in slow, non-reversible deformations that induce pre-damage in both IP and OOP directions [19]. Similarly, previous seismic events may have caused cracking due to deformation demands in either or both IP and OOP directions [20]. Depending on the dominant mode of pre-damage, whether IP or OOP, the SQ loading scenario, which applies pre-damaging in one direction followed by loading in the other, provides the most appropriate representation of such conditions. Alternatively, SC loading can be used to capture the cumulative effects of multiple sequential events that induce damage in stages and influence the subsequent structural response. Other structures may be subjected to a combination of ongoing deformations or loadings concurrent with new actions. For example, wind loading, eccentric gravity effects, or misaligned construction may result in sustained deformations that are quasi-static in duration compared to the new actions [21–23]. With careful consideration of the direction and nature of the predominant ongoing action, these pre-loads and pre-deformations are best represented by the CB loading scenario. Finally, some structures may experience simultaneous IP and OOP loadings, leading to torsional responses as well as combined IP and OOP failure mechanisms [24]. Such

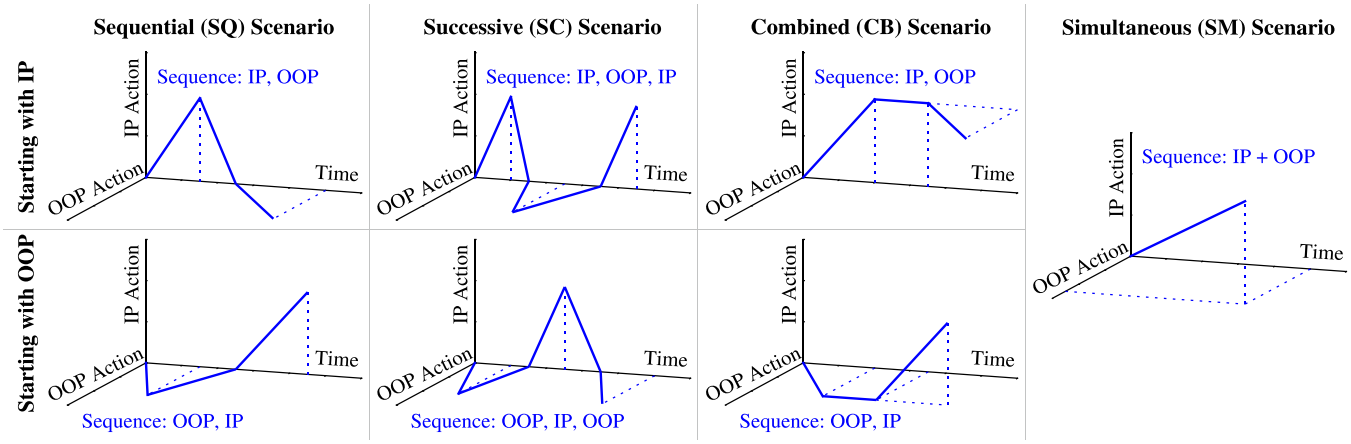

Fig. 1. Examples of different loading sequences used in the study of IP-OOP interaction effects. For the meaning of abbreviations, please refer to the Nomenclature.

conditions are typical of earthquakes, blasts, and impact events. Given the impulsive and short-duration nature of these loadings, they are most accurately replicated using the SM loading scenario.

3. Available research on IP-OOP interaction effects in framed URM walls

This section provides an overview of the experimental and numerical studies published on the IP/OOP and OOP/IP interaction effects in framed URM masonry walls. The approaches include testing wall specimens under laboratory conditions or conducting numerical simulations that represent real-world structures.

Experimental investigations, often conducted in controlled laboratory settings, provide invaluable insights into the actual performance of masonry constructions under different loading scenarios [18,25]. In these tests, lateral loads are usually applied to simulate earthquake-induced forces, returning among others the shear resistance, stiffness degradation, and energy dissipation of the walls [26]. The number of experimental studies on the IP-OOP interaction effects in framed URM walls published until the current year (2025) is depicted in Fig. 2. The list of these experiments is reported in Table 1 along with the most relevant details of each study. It is noteworthy that, as mentioned above, the table reports only tests conducted on unreinforced specimens and specifically under IP-OOP interaction. Hence, while some of the studies may comprise additional experiments performed to investigate the interaction effects in novel or strengthened constructions, or specimens under pure IP or OOP load [17], these tests have not been included in Table 1. In the table, the name Infilled Masonry (IM) refers to panels built within a reinforced concrete (RC) or Steel frame; these differ from Confined Walls (CM), for which the construction of the surrounding frame comes after the masonry of the wall [27].

General observation of Fig. 2 shows that 39 research articles, theses, and conference contributions, reporting the results of experimental campaigns on the effects of IP-OOP interaction in framed URM walls have been published over the past 30 years. A significant increase in interest is observed in the 2010s, during which 85 % of the total research activities have been conducted. It is remarkable that studies on framed walls focusing on IP-OOP interactions, although numerous, constitute only about 10 % of the total experimental data on framed panels [2], with the other 90 % focusing on their response under pure IP or OOP load. The tests have been performed, with variations in the typology of both specimens and loading procedures. The former includes the geometrical scale of the specimens, the presence of openings or internal ties, and geometrical aspects such as height-to-thickness slenderness ratio and length-to-height aspect ratio, while the latter includes changes in the loading sequence and type, vertical stress level, and the level of pre-damage considered. The influence of such characteristics on the wall performance and the IP/OOP and OOP/IP interaction effects is discussed in 4.

The complexity, cost, and limitations in scalability of experimental setups have led to the increasing relevance of numerical modeling as a viable alternative to experimental campaigns to investigate the effects of IP-OOP interactions [5]. Thanks to their versatility and the moderate cost required to set up an analysis, numerical simulations allow for extensive investigations. Besides, they enable the study of parameters that are difficult to control or observe in physical experiments, such as the variations in material properties, boundary conditions, and loading [5]. Fig. 2 illustrates the number of published numerical studies for investigating the interaction effects in framed masonry walls since the very first experimental study was conducted. Moreover, Table 2 lists the relevant information of the framed URM specimens considered in these studies. The smaller number of numerical investigations compared to the experimental ones relates to the structural function of framed walls, which act as secondary elements contributing to the broader stability of the buildings. For this reason, numerical studies rarely focus on their individual behaviors, and use the understandings obtained from experimental studies to directly simulate the interaction effects in complete buildings or multi-bay frames [3,8,9,15,20,28–37]. Since the structural level performance is affected by many variables, from which the isolation of influences from IP/OOP and OOP/IP interactions is a challenge beyond the scope of this study, only the outcomes of 13 works [5,13,16,28,32,38–45] conducted for individual framed walls and multi-bay multi-story frames are included in Table 2 and the discussions of 4.

The numerical works are categorized based on the modeling approach they adopt, following the classification scheme proposed in [46] where different modeling techniques are distinguished based on their approach to the geometrical representation of masonry into Block-Based (BB), Continuum-Based (CoB), and Macro Element (ME) groups. In summary, Block-Based models follow a discrete cracking approach where a discontinuous geometry is assembled by continuum bodies separated by discontinuities that explicitly represent potential crack propagation paths. They use continuum rigid or deformable blocks connected via zero-thickness joints to represent masonry components and failure mechanisms at different scales, allowing them to account for masonry heterogeneity and brick-mortar interactions. They can be further classified into several categories, including, but not limited to, detailed and simplified micro-scale sub-categories. Detailed micro-scale (DMSBB) models, such as [47,48], simulate each masonry unit and mortar layer with separate continuum blocks, and use connectivity elements or contact algorithms to simulate the zero-thickness interaction surface between them [48] and the panel-frame connections. Simplified Micro-Scale Block-Based (SMSBB) models [49–68] lump the mechanical response of both mortar layers and mortar-unit interfaces into zero-thickness elements and virtually extend the masonry units by half

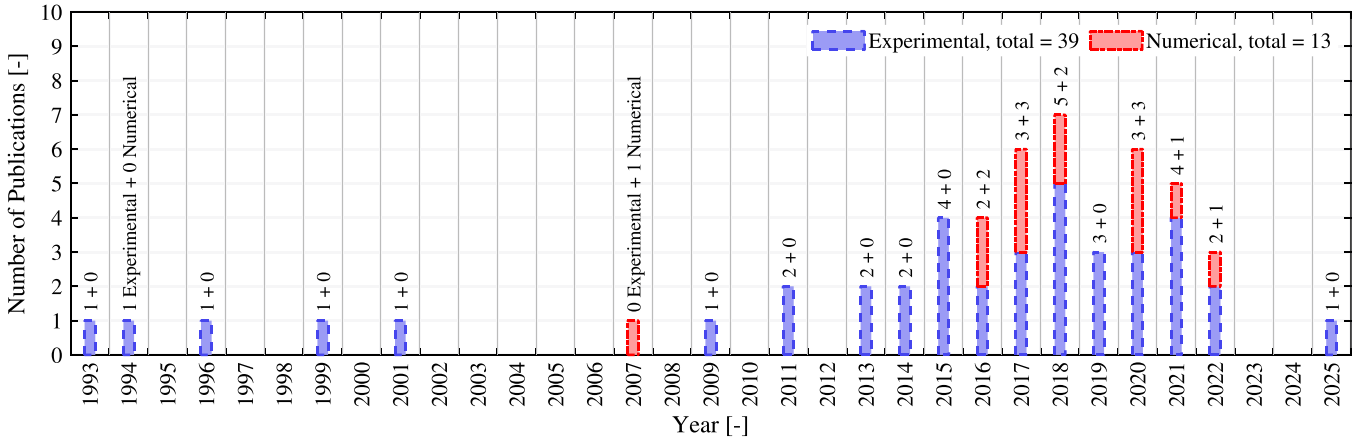

Fig. 2. Number of publications per year focusing on the experimental and numerical study of framed unreinforced masonry walls under IP-OOP interaction effects.

Table 1
Experimental studies regarding the effects of IP-OOP interaction on the response of framed unreinforced masonry walls. For the meaning of abbreviations, please refer to the Nomenclature. Parentheses show the number of specimens with the specific features.

Interaction Scenario	Year	Author(s)	URM Interaction Tests (Number – Type)	Scale (Test/Reality)	Masonry Unit Type	Mortar Type	Masonry Prism Compressive Strength (f'_m) [MPa]	Frame Type	Opening Type	Multi-bay Specimens	Length/Height Aspect Ratio (l/h)	Length/Thickness Slenderness Ratio (h/t)	No. Wythes	Panel Thickness (t) [mm]	Loading Scenario and Sequence	IP Loading (Procedure, Apparatus, Boundary Conditions)	OOP Loading (Procedure, Apparatus, Boundary Conditions)	Vertical Overburden Stress/Strength (Columns + Wall) [%]
IP/OOP	1994	R. Angel et al. [71,72]	2 – IM	1/1	SCLB	1:1:6 (C:L:S)	10.9	RC	–	–	1.5	16.5 (1) 34.1 (1)	1 (1) 0.5 (1)	98 (1) 48 (1)	SQ (IP, OOP)	QSC, FD, DC	QSM, AB, 2WB	4.4 + 0
			3 – IM	1/1	SCLB	1:3 (L:S)	4.5	RC	–	–	1.5	8.7 (1) 16.5 (1) 34.1 (1)	2 (1) 1 (1) 0.5 (1)	143 (1) 98 (1) 48 (1)	SQ (IP, OOP)	QSC, FD, DC	QSM, AB, 2WB	4.4 + 0
			2 – IM	1/1	HCB (V)	1:1:6 (C:L:S) (DHJ)	22.2	RC	–	–	1.5	11.4 (1) 17.7 (1)	1	187 (1) 92 (1)	SQ (IP, OOP)	QSC, FD, DC	QSM, AB, 2WB	4.4 + 0
			1 – IM	1/1	SCLB	1:3 (L:S)	4.6	RC	–	–	1.5	16.5	1	98	CB (IP, OOP)	QSC, FD, DC	QSM, AB, 2WB	4.4 + 0
			1 – IM	1/1	HCB (V)	1:1:6 (C:L:S) (DHJ)	21.5	RC	–	–	1.5	11.4	1	143	CB (IP, OOP)	QSC, FD, DC	QSM, AB, 2WB	4.4 + 0
	1999	R.D. Flanagan R.M. Bennett [73]	1 – IM	1/1	HCLB (H)	1:1:6 (C:L:S)	3	Steel	–	–	1.0	11.2	1	200	SQ (IP, OOP)	QSC, FD, DC	QSLUC, AB, 2WB	0 + 0
			1 – IM	1/1	HCLB (H)	1:1:6 (C:L:S)	3	Steel	–	–	1.0	11.2	1	200	CB (IP, OOP)	QSC, FD, DC	QSLUC, AB, 2WB	0 + 0
	2001	G. Calvi and D. Bolognini [74]	2 – IM	1/1	HCLB (H)	1:1:6 (C:L:S)	1.1	RC	–	–	1.5	23.9	1	115	SQ (IP, OOP)	QSC, FD, DC	QSM, FD, 1WB-B	Not Specified + 0
	2009	D.C. Rai et al. [75]	2 – IM	1/2	SCLB	1:1:6 (C:L:S)	6.6	RC	–	1 (Q)	0.85 (1) 1.7 (1)	22.8	1	59.5	SC (OOP, IP, OOP)	QSC, FD, DC	Dyn, ST, 2WB	20 + 1.5
	2011	M.F.P. Pereira et al. [76]	1 – IM	2/3	HCLB (H)	1:1:6 (C:L:S)	1.3	RC	–	–	2.5	11.3	1	150	SQ (IP, OOP)	QSC, FD, DC	QSM, AB, 2WB	40 + 0
	2011	S. Komaraneni et al. [77]	1 – IM	1/2	SCLB	1:1:6 (C:L:S)	6.6	RC	–	–	1.7	11.0	1	165	SC (OOP, IP, OOP)	QSC, FD, DC	Dyn, ST, 2WB	20 + 1.5
	2013	F. da Porto et al. [78,79]	2 – IM	1/3	HCLB (V)	1:1:6 (C:L:S) (DHJ)	6	RC	–	–	1.6	8.8	1	300	SQ (IP, OOP)	QSC, FD, DC	QSM, WF4PL, 2WB	Not Specified + 0
	2014	S. Hak et al. [80–82]	4 – IM	1/1	HCLB (V)	1:1:6 (C:L:S) (DHJ)	4.6	RC	– (3) D (1)	–	0.5 (3) 1.4 (1)	8.4	1	350	SQ (IP, OOP)	QSC, FD, DC	QSLUC, WF4PL, 2WB	10 + 0
	2014	V. Singhal and D.C. Rai [27]	1 – IM	1/2	SCLB	1:1:6 (C:L:S)	9.2	RC	–	4	0.8	22.8	1	59	SC (OOP, IP, OOP)	QSC, FD, DC	Dyn, ST, 2WB	20 + 1.5
			3 – CM	1/2	SCLB	1:1:6 (C:L:S)	9.2	RC	–	4	0.8	22.8	1	59	SC (OOP, IP, OOP)	QSC, FD, DC	Dyn, ST, 2WB	20 + 1.5
	2015	F. da Porto et al. [83]	3 – IM	1/1	HCLB (H)	1:1:6 (C:L:S)	2	RC	–	–	1.6	17.7	1	120	SQ (IP, OOP)	QSC, FD, DC	QSM, WF4PL, 2WB	40 + 0
	2015	A. Furtado et al. [84,85]	1 – IM	1/1	HCLB (H)	1:1:6 (C:L:S)	0.6	RC	–	–	1.8	15.3	2 (Cav)	150-40-110	SQ (IP, OOP)	QSC, FD, DC	QSLUC, AB, 2WB	0 + 0
	2016	V. Singhal and D.C. Rai [86,87]	1 – IM	1/2	SCLB	1:1:6 (C:L:S)	8.5	RC	W	4	0.8	22.8	1	59.5	SC (OOP, IP, OOP)	QSC, FD, DC	Dyn, ST, 2WB	20 + 1.5
			3 – CM	1/2	SCLB	1:1:6 (C:L:S)	8.5	RC	W (2) W + D (1)	4	0.8	22.8	1	59.5	SC (OOP, IP, OOP)	QSC, FD, DC	Dyn, ST, 2WB	20 + 1.5
	2017	R. Sepasdar [88] and C. Wang [89]	3 – IM	1/2	HCB (V)	1:3:12 (C:L:S)	9.5	RC	–	–	1.4	10.9	1	200	SQ (IP, OOP)	QSM, FD, DC	QSM, AB, 2WB	0 + 0
	2018	O. Onat et al. [90]	1 – IM	1/1	HCLB (H)	1:1:6 (C:L:S)	1.3	RC	–	–	2.5	10.2	1	220	SM (IP + OOP)	Dyn, ST, DC	Dyn, ST, 2WB	10 + 0
	2018	P. Ricci et al. [91]	3 – IM	2/3	HCLB (H)	1:1:6 (C:L:S)	1.8	RC	–	–	1.3	22.8	1	80	SQ (IP, OOP)	QSC, FD, DC	QSM, WF5PL, 2WB	0 + 0
	2018	P. Ricci et al. [92]	3 – IM	2/3	HCLB (H)	1:1:6 (C:L:S)	1.8	RC	–	–	1.3	15.2	1	120	SQ (IP, OOP)	QSC, FD, DC	QSM, WF5PL, 2WB	0 + 0
	2019	C. Butenweg et al. [93,94]	1 – IM	1/1	HCLB (V)	1:1:6 (C:L:S) (DHJ)	3.1	RC	–	–	1.1	6.9	1	365	SC (IP, OOP, IP)	QSC, FD, DC	QSLUC, AB, 2WB	10 + 0
	2019	M.T. De Risi et al. [95]	3 – IM	2/3	HCLB (H)	1:1:6 (C:L:S)	2.4	RC	–	–	1.0	22.8	1	80	SQ (IP, OOP)	QSC, FD, DC	QSM, WF5PL, 2WB	0 + 0
	2019	S.L. Sagar et al. [96]	1 – IM	1/2	SCLB	1:1:6 (C:L:S)	8.1	RC	–	–	1.8	17.1	1	76	SC (OOP, IP, OOP)	QSC, FD, DC	Dyn, ST, 2WB	20 + 1.5
	2020	E. Nasiri and Y. Liu [43]	3 – IM	1/2	HCB (V)	1:1:6 (C:L:S)	17.1	RC	–	–	1.4	10.9	1	90	SQ (IP, OOP)	QSM, FD, DC	QSM, AB, 2WB	0 + 0
	2020	F. Akhoundi et al. [97,98]	3 – IM	1/2	HCLB (H)	1:1:6 (C:L:S)	2.25	RC	–	–	1.5	19	2 (Cav)	80-10-60	SQ (IP, OOP)	QSC, FD, DC	QSLUC, AB, 2WB	40 + 0
	2020	F. da Porto et al. [99]	3 – IM	1/1	HCLB (H)	1:1:6 (C:L:S) (DHJ)	1.2	RC	– (2) D (1)	–	1.6	8.8	1	300	SQ (IP, OOP)	QSC, FD, DC	QSM, WF4PL, 2WB	40 + 0
	2021	G. Santarsiero et al. [100]	1 – IM	1/1	HCLB (H)	1:1:6 (C:L:S)	Not Specified	RC	–	–	1.6	8.7	2 (Cav)	120-100-80	SQ (IP, OOP)	QSC, FD, DC	–, AV, 2WB	10 + 0
	2021	M. Di Domenico et al. [101]	2 – IM	2/3	HCLB (H)	1:1:6 (C:L:S)	1.3	RC	–	–	1.0	15.2	1	120	SQ (IP, OOP)	QSC, FD, DC	QSM, WF5PL, 2WB	0 + 0
	2025	P. Morandi et al. [102]	3 – IM	1/1	HCLB (H)	1:3:12 (C:L:S)	1.1	Composite	–	–	1.3	11	1	120	SQ (IP, OOP)	QSC, FD, DC	Dyn, ST, 2WB	0 + 0
OOP/IP	1993	R.C. Henderson et al. [103]	1 – IM	1/1	HCLB (H)	1:1:6 (C:L:S)	3.3	Steel	–	–	1.2	22.6	1	300	SQ (OOP, IP)	QSC, FD, DC	QSC, FD, 1WB-Ct	0 + 0
	1999	R.D. Flanagan R.M. Bennett [73]	3 – IM	1/1	HCLB (H)	1:1:6 (C:L:S)	3	Steel	–	–	1.0	11.2	1	200	SQ (OOP, IP)	QSC, FD, DC	QSLUC, FD, 1WB-Ct (2) QSLUC, AB, 2WB (1)	0 + 0
	2018	V. Paliraki et al. [104]	1 – IM	1/1	HCLB (H)	1:1:6 (C:L:S)	3.5	RC	–	–	1.3	25.9	1	90	SQ (OOP, IP)	QSC, FD, DC	QSLUC, WF6PL, 2WB	0 + 0
	2019	C. Butenweg et al. [93,94]	1 – IM	1/1	HCLB (V)	1:1:6 (C:L:S) (DHJ)	3.1	RC	–	–	1.1	6.9	1	365	CB (OOP, IP)	QSC, FD, DC	QSM, AB, 2WB	10 + 0

the thickness of the mortar layers [57]. These models can yield similar levels of accuracy as the detailed models, but with lower computational costs. Yet, their application is still limited to the study of the response of individual walls under quasi-static monotonic and cyclic loading [49–68].

Continuum-based approaches consider the masonry structure as one deformable continuum body [69]. Due to the continuity of the elements and the absence of discrete cracking paths, nonlinear behaviors and failures are diffused throughout the volume, following a smeared cracking approach. The continuum body is discretized into relatively bigger elements compared to block-based models, and unit-mortar interactions are implicitly incorporated in the constitutive behavior of the components, leading to fewer degrees of freedom and lower computational demands [46]. The CoB models can be effectively employed to study the local structural responses of unreinforced and reinforced masonry constructions under multi-directional quasi-static and seismic actions.

In macro-element models, different components of a masonry panel are idealized into single or multiple beam-column or strut members connected together via pins or hinges [70]. The behavior of the elements is calibrated based on previous experiments, high-fidelity numerical models, or analytical formulations. Compared to previous groups, these models are more oriented towards using generalized phenomenological behaviors to replicate structural-level responses rather than local failures. At the same time, by simplifying geometry into a reduced number of elements, the computational costs of using these models are significantly reduced. Hence, the macro-element models offer an invaluable engineering tool for the assessment and design of large structures under seismic loads, especially in engineering practices [46].

4. Current findings regarding IP-OOP interaction effects in framed URM walls

This section offers a summary of the key findings of previous experimental and numerical studies on the effects of IP-OOP interaction on the structural behavior of framed masonry walls. The IP-OOP interaction effects are typically measured by comparing the IP or OOP strength and damage patterns of the specimens studied under IP/OOP interaction with those of their reference specimens under pure IP or OOP load of the same type. In addition, stiffness, and deformation corresponding to the initiation of cracking and the 20 % drop in strength (considered as the ultimate deformation capacity) are also compared [81,99]. The ratio between ultimate and cracking deformation is regarded as the indicator of the ductility of the specimen and is occasionally included in the comparisons. It should be noted that the parameters mentioned here are not investigated in every single study and might be missing in some publications. A comprehensive description of each study is omitted due to the large number of experiments. Instead, the influence of various factors such as geometry, material properties, boundary conditions, interaction scenarios, and loading apparatus on the extent of IP-OOP interaction effects is discussed.

The number of tested specimens and simulated walls reported for each study in Table 1 and Table 2 is based on the descriptions provided in their respective publications. However, since parts of the outcomes miss fundamental information necessary to conduct this comparative study, only that part of the data pool with complete and verified

Table 2
Numerical studies regarding the effects of IP-OOP interaction on the response of framed unreinforced masonry walls. For the meaning of abbreviations, please refer to the Nomenclature. Parentheses show the number of specimens with the specific features.

Interaction Scenario	Year	Author(s)	URM Interaction Specimens (Number – Type)	Numerical Modeling Approach	Masonry Unit Type	Mortar Type	Masonry Prism Compressive Strength (f'_m) [MPa]	Frame Type	Opening Type	Multi-bay Specimens	Length/Height Aspect Ratio (l/h)	Length/Thickness Slenderness Ratio (h/t)	No. Wythes	Panel Thickness (t) [mm]	Loading Scenario and Sequence	IP Loading (Procedure, Apparatus, Boundary Conditions)	OOP Loading (Procedure, Apparatus, Boundary Conditions)	Vertical Overburden Stress/Strength (Columns + Wall) [%]	Pre-Damage Levels
IP/OOP	2016	T.Y.P. Yuen et al. [5]	2 – IM	SMSBB	HCLB (V)	1:1:6 (C:L:S)	5.0	RC	– (1) PF (1)	2 (2St – 2Ba)	2.8	8.9	1	300	SM (IP + OOP)	Dyn, ST, –	Dyn, ST, 2WB	0 + 0	4 (2)
	2017	V. Bahreini [39]	4 – IM	SMSBB	SCB	1:1:6 (C:L:S)	13.6	RC	–	–	1.0 (2) 2.0 (2)	30.6	1	92	CB (IP, OOP)	QSM, FD, DC	QSM, AB, 2WB	1.1 + 5.2 (2) 0 + 0 (2)	3 (4)
			2 – IM	SMSBB	SCB	1:1:6 (C:L:S)	13.6	RC	–	–	1.0 (1) 2.0 (1)	30.6	1	92	CB (IP, OOP)	QSM, FD, DC	Dyn, ST, 2WB	1.1 + 5.2	3 (2)
	2018	F. Di Trapani et al. [41]	2 – IM	ME	HCB (V) (DHJ) (1) SCLB (1)	1:1:6 (C:L:S)	4.5 (1) 2.3 (1)	RC	–	–	1.5	17.7 (1) 34.1 (1)	1	92 (1) 48 (1)	SQ (IP, OOP)	QSC, FD, DC	QSM, WFMiPL, 2WB	4.4 + 0	4 (2)
	2018	F. Mazza [42]	3 – IM	ME	HCLB (H)	1:1:6 (C:L:S)	0.4	RC	–	–	1.5 (2) 1.25 (1)	13.8 (2) 16.6 (1)	2 (Cav)	120-50-120	SM (IP + OOP)	QSC, FD, DC	QSC, WFMiPL, 2WB	2.8 + 0 (1) 15.9 + 0 (1) 24.8 + 0 (1)	1 (3)
			3 – IM	ME	HCLB (H)	1:1:6 (C:L:S)	1.5	RC	–	–	1.5 (2) 1.25 (1)	41.2 (2) 50.0 (1)	1	80	SM (IP + OOP)	QSC, FD, DC	QSC, WFMiPL, 2WB	2.8 + 0 (1) 15.9 + 0 (1) 24.8 + 0 (1)	1 (3)
			3 – IM	ME	HCLB (V)	1:1:6 (C:L:S)	3.9	RC	–	–	1.5 (2) 1.25 (1)	11.0 (2) 13.3 (1)	1	300	SM (IP + OOP)	QSC, FD, DC	QSC, WFMiPL, 2WB	2.8 + 0 (1) 15.9 + 0 (1) 24.8 + 0 (1)	1 (3)
	2020	E. Nasiri and Y. Liu [43]	9 – IM	SMSBB	HCB (V)	1:1:6 (C:L:S)	8.0 (3) 12.0 (3) 16.0 (3)	RC	–	–	0.8 (3) 1.0 (3) 1.3 (3)	18 (3) 14 (6)	1	200	SQ (IP, OOP)	QSM, FD, DC	QSM, AB, 2WB	0 + 0	4 (9)
			2 – IM	SMSBB	HCB (V)	1:1:6 (C:L:S)	12.0	RC	–	–	1.0	18.6 (1) 28 (1)	1	150 (1) 100 (1)	SQ (IP, OOP)	QSM, FD, DC	QSM, AB, 2WB	0 + 0	4 (2)
			3 – IM	SMSBB	HCB (V)	1:1:6 (C:L:S)	12.0	RC	–	–	0.8 (1) 1.0 (1) 1.3 (1)	18 (1) 14 (2)	1	200	SQ (IP, OOP)	QSC, FD, DC	QSM, AB, 2WB	0 + 0	4 (3)
	2020	X. Wang et al. [44]	7 – IM	SMSBB	SCLB	1:1:6 (C:L:S)	4.9 (1) 10.9 (5) 16.9 (1)	RC	–	–	0.75 (1) 1.5 (5) 2.3 (1)	17 (1) 26 (1) 34 (5)	1	48 (5) 63 (1) 96 (1)	SQ (IP, OOP)	QSM, FD, DC	QSM, AB, 2WB	4.4 + 0	2 (7)
	2020	L. Cavaleri et al. [45]	3 – IM	CoB	SCLB	1:1:6 (C:L:S)	4.6	RC	–	–	0.9	8 (1) 12 (1) 24 (1)	1	300 (1) 200 (1) 100 (1)	SQ (IP, OOP)	QSC, FD, DC	QSM, AB, 2WB	4.4 + 0	5 (3)
			3 – IM	CoB	SCLB	1:1:6 (C:L:S)	4.6	RC	–	–	0.6	12 (1) 18 (1) 36 (1)	1	300 (1) 200 (1) 100 (1)	SQ (IP, OOP)	QSC, FD, DC	QSM, AB, 2WB	4.4 + 0	5 (3)
			3 – IM	CoB	SCLB	1:1:6 (C:L:S)	3.0	RC	–	–	0.9	8 (1) 12 (1) 24 (1)	1	300 (1) 200 (1) 100 (1)	SQ (IP, OOP)	QSC, FD, DC	QSM, AB, 2WB	4.4 + 0	5 (3)
			4 – IM	CoB	SCLB	1:1:6 (C:L:S)	3.0	RC	–	–	0.6	12 (2) 18 (1) 36 (1)	1	300 (2) 200 (1) 100 (1)	SQ (IP, OOP)	QSC, FD, DC	QSM, AB, 2WB	4.4 + 0	5 (4)
	2021	B. Pradhan et al. [13]	18 – IM	ME	HCLB (V)	1:1:6 (C:L:S)	1 (3) 2 (3) 3 (3) 4 (3) 5 (3) 6 (3)	RC	–	–	1.0	8.6 (6) 13 (6) 26 (6)	1	300 (6) 200 (6) 100 (6)	SQ (IP, OOP)	QSC, FD, DC	QSM, WFMiPL, 2WB	0 + 0	7 (18)
			6 – IM	ME	HCLB (V)	1:1:6 (C:L:S)	1 (3) 6 (3)	RC	–	–	1.5	8.6 (2) 13 (2) 26 (2)	1	100 (2) 200 (2) 300 (2)	SQ (IP, OOP)	QSC, FD, DC	QSM, WFMiPL, 2WB	0 + 0	7 (6)
			6 – IM	ME	HCLB (V)	1:1:6 (C:L:S)	1 (3) 6 (3)	RC	–	–	2.0	8.6 (2) 13 (2) 26 (2)	1	100 (2) 200 (2) 300 (2)	SQ (IP, OOP)	QSC, FD, DC	QSM, WFMiPL, 2WB	0 + 0	7 (6)
OOP/IP	2007	A. Hashemi and K.M. Mosalam [38]	1 – IM	CoB	SCLB	1:1:6 (C:L:S)	2.0	RC	–	–	0.7	25.4	1	100	CB (OOP, IP)	QSM, FD, DC	QSM, AB, 2WB	0 + 0	5 (1)
			8 – IM	ME	SCLB	1:1:6 (C:L:S)	1.0 (1) 2.0 (6) 4.0 (1)	RC	–	–	0.7	20.6 (1) 25.4 (6) 46.3 (1)	1	56 (1) 100 (6) 126 (1)	CB (OOP, IP)	QSM, FD, DC	QSM, WFMiPL, 2WB	0 + 0	12 (2) 11 (2) 9 (3) 8 (1)
	2016	T.Y.P. Yuen et al. [5]	3 – IM	SMSBB	SCLB	1:1:6 (C:L:S)	5.0	RC	– (1) D (1) PF (1)	–	2.2	24.1	1	115	CB (OOP, IP)	QSM, FD, DC	QSM, AB, 2WB	5 + 1	3 (3)
	2016	J. Kong et al. [16]	1 – IM	SMSBB	SCLB	1:1:6 (C:L:S)	11.5	RC	–	–	1.5	16.5	1	98	CB (OOP, IP)	QSM, FD, DC	QSM, AB, 2WB	4.4 + 0	4 (1)
	2017	M. Doná et al. [28]	12 – IM	ME	HCLB (V) (6) HCLB (H) (6)	1:1:6 (C:L:S) (DHJ)	6.0 (6) 4.5 (6)	RC	–	4 (2St – 5Ba) 4 (3St – 2Ba) 4 (5St – 2Ba)	1.6 (6) 1.5 (6)	9.5 (6) 25.6 (6)	1	300 (6) 115 (6)	SM (IP + OOP)	QSM, FD, –	QSM, WFMiPL, 2WB	0 + 0	4 (12)
	2017	M. Di Domenico et al. [40]	1 – IM	ME	HCLB (H)	1:1:6 (C:L:S)	2.4	RC	–	–	1.3	28.0	1	100	SM (IP + OOP)	Dyn, ST, DC	Dyn, ST, 2WB	0 + 0	22 (1)
	2022	M. Doná et al. [32]	8 – IM	ME	HCLB (H)	1:1:6 (C:L:S)	1.1	RC	–	2 (2St – 4Ba) 2 (3St – 2Ba) 2 (3St – 1Ba) 2 (6St – 2Ba)	1.5	26.1	1	115	SM (IP + OOP)	QSM, FD, –	QSM, WFMiPL, 2WB	0 + 0	5 (8)

information is used herein. The entire findings of each study are not re-iterated in the text, as parts of the outcomes from different campaigns overlap. For the sake of brevity, the findings from experimental tests are established as the primary references for investigating IP-OOP interaction effects, and the results of numerical investigations are used as complementary information to fill in the gaps or address topics not examined through experimentation. Accordingly, the findings of experimental studies are regarded as the most representative of the actual behavior of framed walls and are critically analyzed. Numerical studies, having typically calibrated their models against specific experimental benchmarks [13,41–43,45,51,89], are considered to provide non-generalizable auxiliary insights and are referenced primarily in cases where experimental data are limited or unavailable. It should be noted that only the outcomes and observations already reported or visualized in the original publications are reiterated and cross-compared in this manuscript. In other words, no new interpretations or post-processing of the reviewed data are introduced. All observations and comparisons are strictly based on information available in the cited works. However, to maintain the readability and flow of the text, individual citations are not provided at the end of each sentence discussing those works.

Studies of the influence of different strengthening techniques, such as the use of textile-reinforced mortar joints [105,106], surface reinforcement with steel [76] or regular [78,83] and fiber-reinforced [78,79,83,96,107] plaster or insulation [105,106], bed joint reinforcement [90,108], head and bed joint reinforcement [99], use of cementitious matrix [96], etc., on IP-OOP interaction effects are reported for the sake of completeness; however, only the outcomes of the experiments conducted on unreinforced specimens are discussed, while the parts regarding the impact of strengthening are disregarded. The endeavors on the development of novel construction techniques, especially in framed walls, such as the use of sliding joints between masonry units [82,109] or special connections between frames and decoupled infills [7,94,110], are also excluded. Finally, the effect of different parameters on the behavior under pure IP or OOP loading is not discussed when it does not contribute to understanding the interaction effects.

Overall, 85 % of the tests, including the 12 with a starting OOP loading [27,75,77,86,87,96] and the 1 under simultaneous IP and OOP loading [90] as well as 70 % of numerical simulations [13,41–43,45,51,89] focus on the effects of IP/OOP interaction rather than OOP/IP interaction. This is justified by the practical limitations of experimental settings and the lack of data to validate numerical OOP/IP simulations [16]. Moreover, studies have shown that prior low-to-moderate OOP damage in framed panels has only minor effect on the IP behavior [73,103]. Finally, common failures observed in framed URM walls during earthquake events are in the OOP direction, which is highly sensitive to IP pre-damage with cracks propagating through the entire thickness of the wall along the crack paths, calling for more focus on IP/OOP interaction effects [2,17]. In the next subsections, first, the findings on the influence of IP/OOP interaction on OOP behavior are reported, and then the 4 experimental [73,93,103,104] and 6 numerical [5,16,28,32,38,40] studies focusing on the IP response under the influence of OOP/IP interaction are discussed.

4.1. *Effects of IP response on the OOP wall behavior (IP/OOP interaction)*

Although IP/OOP interaction effects can arise from different sources of IP action, such as settlement [111], the current studies in the literature primarily focus on interactions caused by seismic actions, i.e. IP lateral actions simulating the effects of earthquakes. Fig. 3 shows the outcome of the experimental investigations of IP/OOP interaction

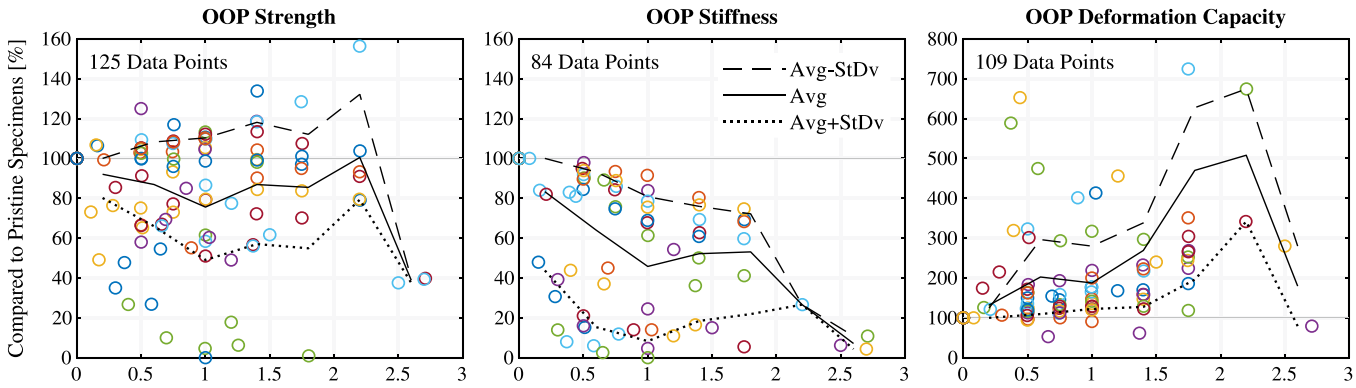

Fig. 3. Overview of data points collected from the outcomes of experimental investigations on the effects of IP/OOP interaction on OOP behavior of framed URM walls. For the meaning of abbreviations, please refer to the Nomenclature.

effects in framed URM walls in the form of changes in the OOP strength, stiffness, and deformation capacity. The y-axis in the sub-figures represents the ratio of OOP strength, stiffness, or deformation capacity of each specimen to that of its pristine counterpart. The varying parameter illustrated in each sub-figure is indicated in bold text above the corresponding sub-figure area. Since the reviewed studies adopt different loading scenarios, the magnitude of IP action (x-axis in the figure) may represent pre-damage, pre-deformation, or simultaneous deformation, depending on the specific experimental protocol. To enhance visual clarity and readability, the axis titles are not repeated for each sub-figure. Instead, the y-axis title is placed on the right-hand side of the sub-figures, and a single x-axis title is provided below the bottom row. The average (Avg), 16th percentile (Avg+StDv), and 84th percentile (Avg+StDv) of the data at different IP action levels are shown in each subfigure via solid, dotted, and dashed lines respectively. The lines are generated by calculating the statistical information of data points within IP drift intervals of 0.4 % (i.e., 0–0.4 %, 0.4–0.8 %, 0.8–1.2 %, etc.) and connecting them together to approximate the trend of changes in OOP performance.

The data points, shown with colored hollow circles, are extracted either directly by collecting quantified interaction effects reported in the publications listed in Table 1 or by digitizing and interpreting the interaction effects from their visualized outputs. Regarding OOP strength, values are taken either as the peak capacity of specimens under quasi-static loading or as the highest applied loading intensity in cases of dynamic testing. For stiffness data, changes in the elastic stiffness of the specimens are considered. Several definitions of elastic stiffness are available in the literature. In this review, for quasi-static tests, elastic stiffness is defined as the secant stiffness, computed from the slope of the force-displacement curve at 70 % of the peak force resistance, following the approach in [81]. For dynamically tested specimens, stiffness changes are assumed proportional to the square of the change in the fundamental frequency, following [90,100,112]. For deformation capacity, not only do different studies have different definitions, but also the definition varies by loading type. In this review, in quasi-static tests, the deformation corresponding to a 20 % strength drop is used for specimens exhibiting softening behavior, as done in [81], while for those without observable softening the final recorded deformation is used. In dynamic tests, the maximum deformation recorded during the loading history is considered. It should be noted that maximum deformations are consistently taken from the location of peak displacement in the specimens, typically at mid-height and mid-length, due to the use of two-way bending or one-way beam-like OOP boundary conditions across all experiments.

The data points correspond exclusively to specimens for which experimental data of their pristine counterparts under pure OOP loading and no interaction effects are available. Among all studies reviewed in this manuscript, the twelve experimental specimens reported in [78–83, 99] do not fully meet this criterion. However, 6 of these specimens are still included in the figure. For 3 specimens [80–82], the original publications define the expected pristine behavior based on the response of the specimen with the lowest level of pre-damage. For another 3 specimens [99], the expected pristine response is derived from analytical interaction curves. As a result, only 2 specimens from [78,79], 3 specimens from [83] and 1 specimen from [80–82] are excluded from the figure.

Fig. 3 illustrates a significant scatter in the experimental outcomes, particularly regarding the changes in OOP strength, primarily due to the differences among the specimens tested in each study. Nevertheless, general trends can be observed. Specifically, the increase in IP pre-damage, pre-deformation, and simultaneous IP deformation is shown to reduce OOP strength and stiffness, while increasing the OOP deformation of walls.

Experimental works suggest that if IP pre-damage or pre-deformation is below a critical intensity corresponding to the observation of first IP damage, interaction effects do not appear, and the OOP behavior will remain similar to that of pristine specimens purely loaded in the OOP direction [73,91,98]. In fact, low intensity IP pre-load or deformation, wherein the specimen remains in the elastic phase of its IP response, might as well improve the OOP strength and stiffness by developing compressive struts in the wall and enhancing the OOP arching actions [51,101]. Different IP pre-damage or pre-load thresholds instigating the effects on OOP response are reported in experimental and numerical studies, yet there is a large scatter in the observations, leading to the proposition of thresholds ranging between 0 % and 0.65 % IP drifts (see 5.2).

Larger IP pre-damage or pre-deformation leads to a reduction in both strength and stiffness in the OOP direction, as well as to an increase in deformation at cracking, peak strength, and ultimate capacity points. The changes become more severe with the progression of pre-damage or pre-deformation [88,95,98]. This occurs not only because of the reduced integrity of the panel, but also due to the change of boundary conditions, such as the formation of gaps at the frame/panel interface, and the frame stiffness reduction in case of concrete cracking or steel yielding [76]. Moreover, the amount of energy dissipation during OOP deformation decreases in the case of IP pre-damage or pre-deformation, as the re-opening of cracks developed during IP loading requires less energy [98]. Although the location of damage caused by IP actions can also influence the extent of IP/OOP interaction effects, this aspect is not adequately explored in the available studies, as the majority of them consider IP double-clamped and OOP two-way bending boundary conditions for the walls [74].

Similar outcomes are observed when the effect of IP pre-damage or pre-deformation on the development of OOP failure modes is discussed. Low pre-damage causes new local failures at the early phases of the OOP loading in certain wall regions that would not be damaged otherwise

[80,93]. However, the subsequent cracking during OOP response is not influenced by those minor damages [98]. Under larger IP pre-damage or pre-deformation conditions, OOP cracks are observed to propagate along the same cracks that developed during the previous IP loading phase, as less force is required to re-open such cracks [71,86,87]. Minor purely OOP cracks might form then only at the final OOP loading stages [71]. In general, the interaction effects gradually diminish, and the walls reach a stable state with no further performance deterioration after exceeding a certain amount of IP pre-damage [74], maintaining a residual capacity in the OOP direction and continuing to contribute to the structural response [90]. On the other hand, walls pre-loaded or pre-deformed in the IP direction exhibit a progression of OOP behaviors similar to those of pre-damaged walls, yet with a faster deterioration in OOP performance for larger IP pre-load and pre-deformation [51,101].

The severity of the interaction effects at a certain pre-damage or pre-deformation level varies with the geometrical and mechanical attributes of the walls [17]. The following subsections discuss the outcomes of previous studies based on specimen characteristics and test setups to identify the effect of different factors on the IP/OOP interaction effects.

4.1.1. Specimen configurations

The experimental and numerical studies on the effect of IP/OOP interaction are classified in this section, as depicted in Fig. 4, based on the following configurations: wall type (Fig. 4.A), number of bays (Fig. 4.B), and presence of openings (Fig. 4.C). More than 90 % of the framed masonry experimental specimens are formed of infilled panels, and only 6 confined walls are studied in one campaign [27,86]. A similar noticeable absence of data for IP/OOP interaction effects is exhibited in multi-bay specimens and walls with openings. The 6 CM and 3 IM walls of [27,75,86] are the only multi-bay specimens investigated. These panels have the same geometry as the single-bay specimens tested in the same experimental campaign, but partitioned into 8 double- [27,86] and 1 quadruple-bay [75] panels via vertical and horizontal concrete elements. Notably, 2 of the double-bay CM [86] employ vertical indentation, known as toothing, to improve the connection between the masonry panels and the vertical concrete members. Moreover, all the 8 double-bay [27,86] specimens are constructed via similar materials. While the focus on single-bay specimens is primarily due to financial and equipment constraints, the prevailing presence of walls lacking opening highlights the need for a thorough understanding of more complicated configurations. Only 6 panels with opening are tested [80,86,99] including 3 CM walls with two symmetrical windows each, 2 IM walls with a door at the middle of each [80,99], and 1 CM wall [86] with a door and a window. The CM specimens utilize vertical and horizontal ties around the openings [86], while the IM panels are tested without such confinement around windows and doors. Preti et al. [109] and Milanesi et al. [82] investigate two additional specimens with door openings but built with new construction techniques and not adhering to common unreinforced masonry building practices. Finally, numerical studies do not include instances of multi-bay specimens or specimens with openings.

Very limited data is available regarding the IP/OOP interaction effects in CM and multi-bay specimens. Nevertheless, the data available in [27,75,86] and illustrated in Fig. 5 offer interesting insight. The use of internal tie elements and columns to divide the panels into multiple bays helps to mitigate OOP drifts and improves IP response and energy dissipation, thus delaying OOP failures to higher IP damage levels [27,75,86]. However, it should be noted that internal ties are shown to also cause localized stress concentrations, which can trigger premature in-plane damage [113]. The single-bay CM panel, tested with a strong frame [65,67], demonstrates better OOP stability after IP loading than the tested IM panels, with its collapse delayed to a higher pre-damage level (2.2 % compared to 1.2 %), accompanied by smaller variations in OOP stiffness. Similar conclusions are drawn when comparing the double-bay CM specimen from the same campaign with its IM counterpart. CM specimens also exhibit distinctive failure patterns when compared to IM specimens, owing to different construction methods. While IM walls undergo significant OOP deflection, with the development of an arching action after the last IP pre-damage level, leading to overturning and consequent collapse, CM walls do not show large OOP deformation, and their failure appears in form of diagonal cracks extended from the middle of the panels to the corners and plastic deformation at the column ends. In fact, CM walls exhibit better composite action with the frame and behave more like a shear wall, delaying the risk of OOP collapse to the highest pre-damage levels. The tests of [27] indicate that the coupling of tie elements is more effective with CM walls, since horizontal and vertical cracks may develop at the masonry/concrete intersections in IM walls, leading therefore to collapse at lower IP damage levels. Moreover, the use of toothing between panels and vertical concrete members helps prevent the concentration of cracks and compressive failure at mid-height of the columns. Instead, damage spreads more evenly across the surface, leading to lower chances of local failures and enhancing OOP stability. Given the fundamental differences in how CM and IM respond to interaction effects, and considering the limited number of experimental investigations focused on CM, further research, particularly experimental, is essential to achieve a more comprehensive understanding of CM wall behavior. Such studies would also yield reliable benchmarks for the calibration and validation of numerical models.

An evident knowledge gap is also observed regarding the influence of

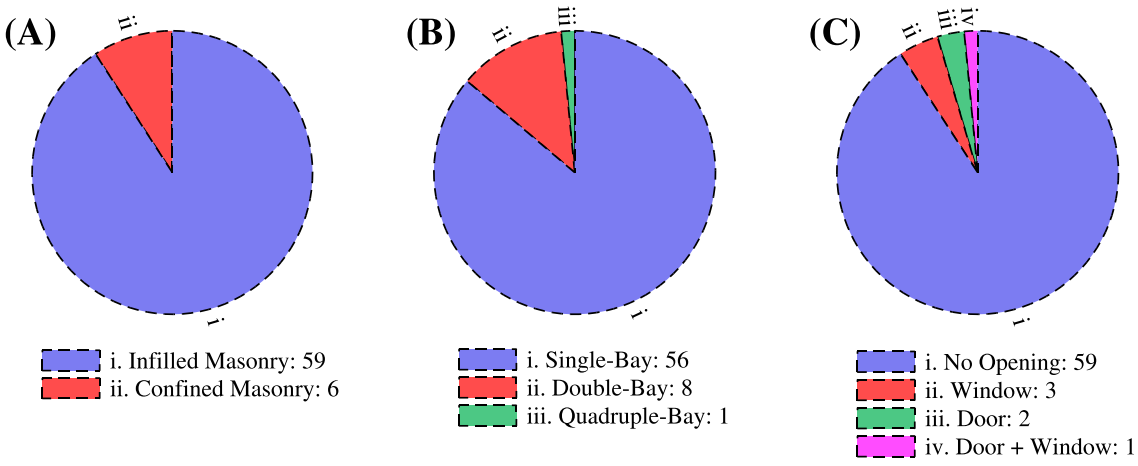

Fig. 4. Categorization of URM framed walls experimentally studied for the IP/OOP interaction effects based on type of specimen (A), number of bays (B), and presence of openings (C). The number of experimental specimens in each category is written in the legends.

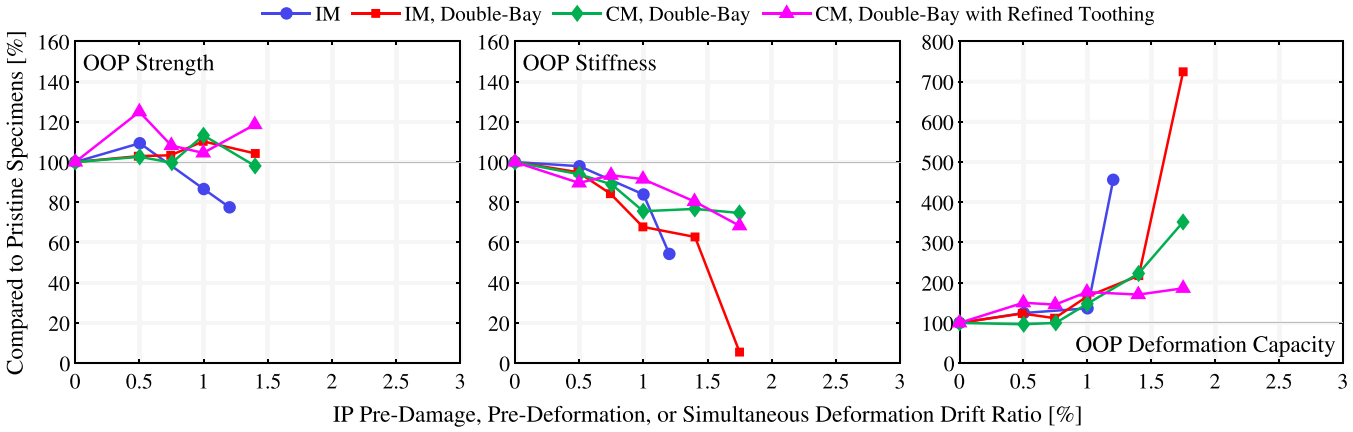

Fig. 5. Example results of IP/OOP interaction effects in walls tested with different types and configurations. The data are extracted from [27,75,86]. For the meaning of abbreviations, please refer to the Nomenclature.

openings on IP/OOP interaction effects. Information regarding the experiment of [80,81] on the IM wall with a full-height door opening is not available and only the results of its IP testing are reported in [114]. Examples of the available experimental data are shown in Fig. 6. Only 1 other IM wall with a door opening is tested by [99] and exhibits good OOP capacity post-IP damage, showing OOP strength reduction only at a high IP pre-damage level, like the reference wall without opening. This low sensitivity to openings is because the propagation of cracks in the opening wall divides each pier into smaller portions that, instead of simply falling off the wall, interlock and maintain the overall OOP strength of the wall [115]. The double-bay IM specimen with window openings from [27,86,87] does not show any higher OOP vulnerability compared to its counterpart with no opening, maintaining stability at even higher IP damage levels (2.2 % IP drift compared to 1.4 %). The main difference consists of a change in IP deformation, with rocking motion of the pier between the openings and significant cracks at the window corners. Similarly, the walls without openings tested by [99] show ductile response with increased OOP deformation capacities after IP pre-damage compared to pristine walls, whereas the wall with the full-height opening exhibits no changes in its OOP deformation capacity post-IP damaging. The latter is related to crushing at the pier corners, aggravated by diagonal cracks from IP loading [99]. Another contributing factor to the greater vulnerability of the wall with an opening is cited as the reduced contribution of the horizontal arching mechanisms to the OOP response due to the presence of a full-height opening, which also separates the left and right piers and causes them to act independently. It is noted in [99] that a lintel and a small spandrel above the opening can significantly mitigate the effect of IP pre-damage: the lintel allows for the simultaneous activation of piers and spandrel, leading to a more homogeneous crack distribution, similar to that of a specimen without openings. Also, for CM specimens, [86,87] observe that the use of confining elements around the openings significantly reduces the negative consequences of the IP/OOP interaction effects. Continuous tie-beams at the top and bottom of the windows are most effective, distributing the cracks uniformly, and maintaining OOP strength and ductility even after severe IP pre-damage (2.2 % IP drift). It should be noted that the middle pier between the door and window in one of the CM panels exhibits significant distortion at an IP pre-damage level above 1 % IP drift, highlighting the need for strengthening.

4.1.2. *Panel geometry*

This section summarizes the outcomes of the IP/OOP interaction investigations, considering variations in terms of specimen scale, number of wythes, IP length-to-height aspect ratio (l/h), OOP height-to-thickness slenderness ratio (h/t), and panel thickness (t).

Regarding the scale of the investigated specimens, although the many of the tests are conducted on full-scale specimens, a significant number involve scaled specimens, with 21 half-scale [27,43,75,77,86,88,89,96,98] and 12 two-thirds-scale [76,91,92,95,101] panels (see Fig. 7.A) due to limitations of testing facilities. As regards the thickness of the specimens, Fig. 7.A shows that 87 % of the tested specimens are constructed in a single-leaf, single-wythe configuration, as framed walls are commonly built in practice. The specimens of Angel et al. [71] include 2 half-wythe and 1 double-wythe panels. The half-wythe walls

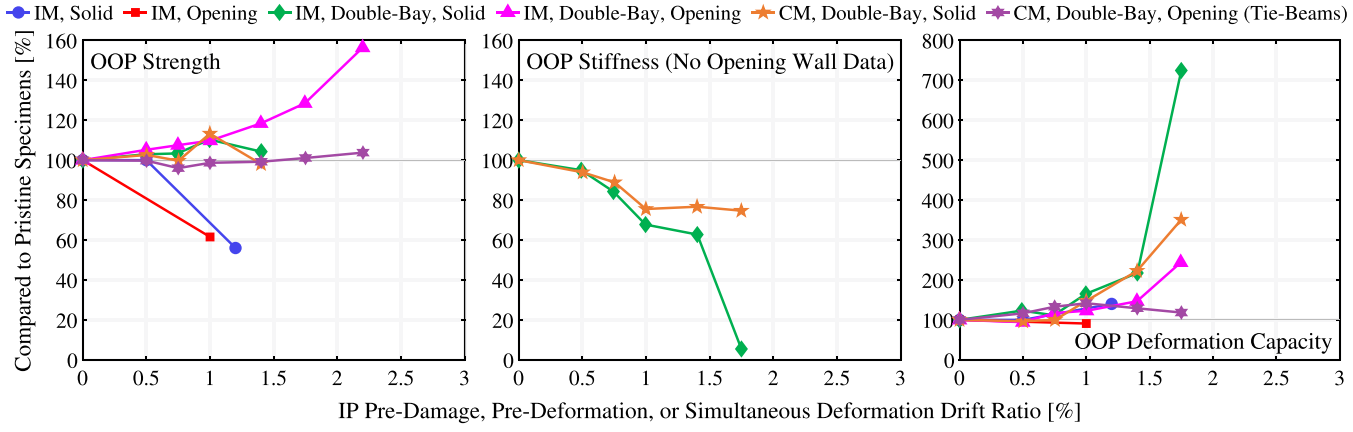

Fig. 6. Example results of IP/OOP interaction effects in walls tested with and without window opening. The data are extracted from [27,86,87,99]. For the meaning of abbreviations, please refer to the Nomenclature.

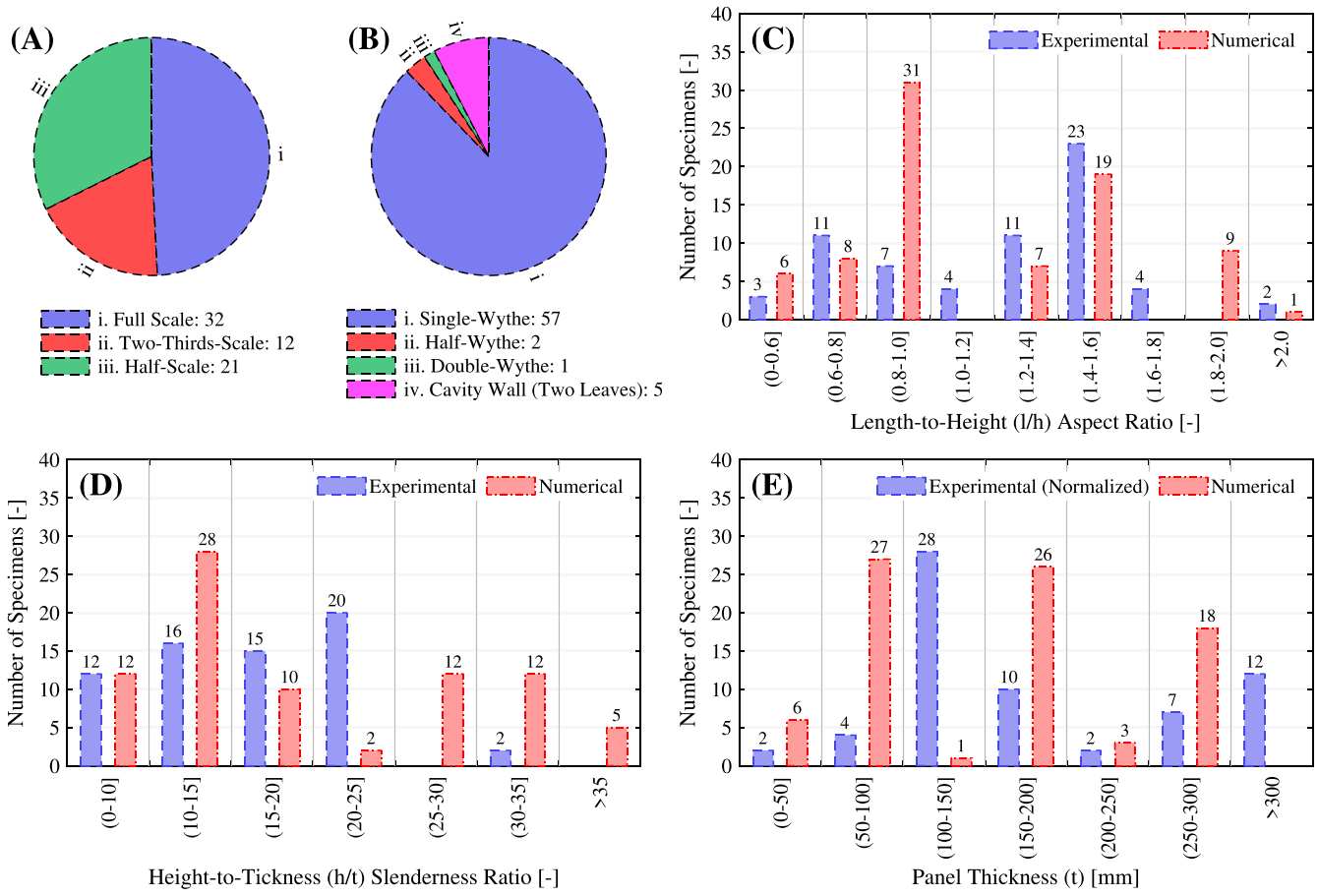

Fig. 7. Geometrical variations explored in experimental and numerical studies of IP/OOP interaction effects in framed URM walls: scale (A) and number of wythes (B) in experimental specimens, and aspect ratios (C), slenderness ratios (D), and thicknesses (E) of experimental and numerical specimens. Thicknesses of experimental specimens are normalized to the 1:1 full scale for direct comparison with those of numerical specimens.

are constructed using bricks that are split in half in their thickness direction. A total of 5 double-leaf cavity walls with a single-wythe inner wall and a single-wythe veneer, with no in-between connection, are tested in [85,98,100]. Specifically, the inner leaf of all 5 specimens is first loaded in the IP direction, while both of their leaves are then tested in the OOP direction.

The l/h aspect ratio has a considerable influence on the response of the walls to IP loading, while the h/t slenderness ratio is of primary importance for the OOP response. According to Fig. 7.C and Fig. 7.D, a diverse range of geometrical configurations are studied, with aspect ratios spanning between 0.5 and 2.5 and slenderness ratios ranging from 6.9 to 50.0. Both figures show satisfactory distribution between different l/h and h/t values, with experimental data missing only at the extremes (l/h>1.8 and h/t > 25). The numerical studies generally focus on squatter (0.6 <l/h<1.0) and less slender panels (5.0 <h/t < 20.0); they also generate data for walls with high slenderness ratios (h/t > 30). A categorization is made based on the thickness of the panels in Fig. 7.E. Since many scaled specimens have been tested, comparing the raw geometrical dimensions is inconclusive [92]. Hence, the thickness of the experimental specimens is normalized to the full (1:1) scale. Previous studies established a thickness of 200–250 mm as a threshold to distinguish between thick and normal walls [17]. It can be observed that all reasonable variations of the normalized thicknesses are adequately covered, except for experimental tests conducted on thin panels with normalized thicknesses less than 100 mm. Nevertheless, this gap is compensated for in numerical campaigns.

Regarding scale effects, none of the existing studies investigate full-scale specimens alongside their small-scale counterparts. As a result, the influence of scale on interaction effects remains unreported and in need of future research. The experimental studies also report no sensitivity of the IP/OOP interaction effects due to the presence of a cavity, or the number of wythes. However, the numerical work conducted in [42] to investigate the structural response of walls under simultaneous cyclic IP/OOP loading reveals a larger and faster reduction in OOP strength and stiffness for the modelled cavity wall compared to a single-wythe single-leaf wall with similar thickness and geometry under the same loading conditions. However, the presence of the cavity might not be the primary cause of the reported differences. Each individual leaf in the cavity wall has a thickness less than half the thickness of the original single-wythe wall. Therefore, each leaf, being more slender, is expected to have been more sensitive to IP/OOP interactions individually as explained in the next paragraph.

The slenderness ratio of the panels is shown to greatly influence the IP/OOP interaction [101], although the conducted investigations lead to contradictory conclusions. It is stated in [80] that thicker walls experience less damage compared to thin walls at different IP drift levels, resulting in lower OOP strength reduction. Moreover, according to [71], horizontal and vertical OOP arching effects are less activated in more slender walls, which results in reduced OOP stability and increased consequences of the IP/OOP interaction. Examples of experimental data regarding interaction effects in walls with different geometries are illustrated in Fig. 8. Supporting the above observations, the tests of [91, 92] on 2 (l/h=1.3) squat walls with different slenderness (h/t = 15.3 and 22.9) show faster degradation in the OOP performance in slender walls. However, the experiments of [71] and [74] contradict the above findings, as no prominent difference is observed between the progression of interaction effects in 2 of their walls with identical aspect ratios (l/h=1.5) and different thicknesses (h/t = 34.1 and 23.9, respectively).

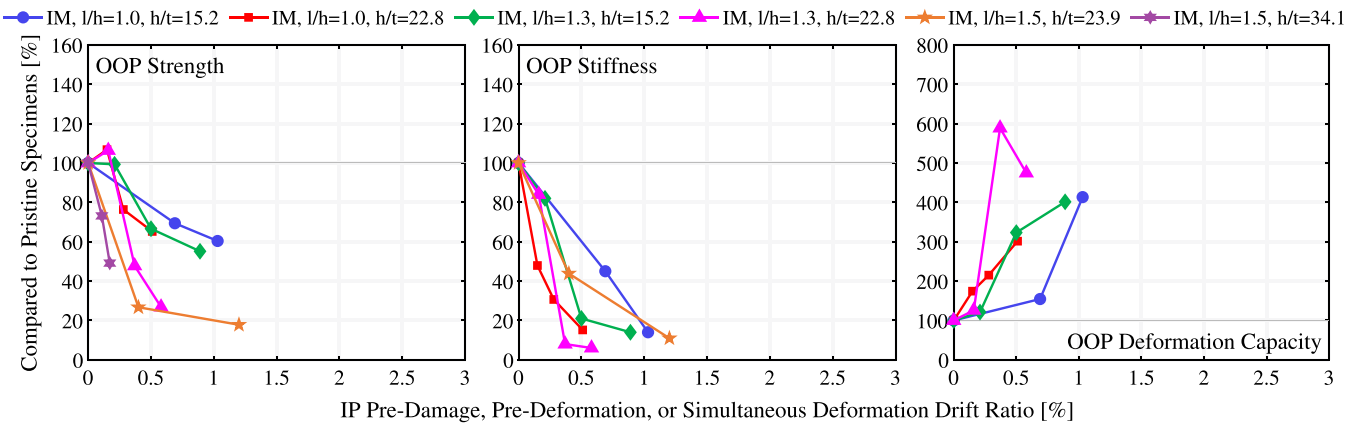

Fig. 8. Example results of IP/OOP interaction effects in walls tested with different aspect ratios and slenderness ratios. The data are extracted from [71,74,91,92]. For the meaning of abbreviations, please refer to the Nomenclature.

As justification, [101] propose that the slenderness ratio influences the IP/OOP interaction effects only when it is lower than a threshold value, above which the OOP arching effects are completely eliminated. The numerical study in [44] on walls similarly squat as those of [71] and [74] (l/h=1.5) and different aspect ratios (h/t = 17.0, 26.0, and 34.0) confirms the existence of such threshold. The mid-slender wall (h/t = 26.0) shows larger OOP strength and stiffness drop compared to the thicker wall (h/t = 17.0). However, its progression of OOP response degradation cis similar to the thinner wall (h/t = 34.0), implying the presence of a slenderness threshold between 17 and 26. Similarly, the numerical study of [13] on walls with different material properties with varying slenderness ratios (h/t = 26, 13, and 8.6), shows higher sensitivity of the most slender walls (h/t = 26) to IP pre-damage whereas the other two walls are similarly affected by IP/OOP interactions. The numerical studies in [43] contradict the presence of such a threshold, as the difference in the trend of IP/OOP interactions in 3 square walls (l/h=1.0) with different slenderness ratios (h/t = 14, 18.6, and 28) is not significant. It is noteworthy to elaborate that the lower sensitivity of the square walls of [43] to the variation of slenderness ratio might have arisen from the effect of aspect ratio, as discussed in the following. The discrepancies between the observations of different studies warrants more investigation into the understanding of the influence of slenderness ratio on interaction effects. Especially, more experiments on specimens with low thicknesses are needed to better identify the presence of the threshold proposed by [101].

Regarding the influence of aspect ratio on the IP/OOP interaction effects, [101] suggest that square walls (l/h=1.0) are less prone to IP/OOP interaction effects. In the experiments of [91,95] on 2 slender walls (h/t = 22.8) with different aspect ratios (l/h=1.3 and 1.0), the squat wall shows an OOP strength reduction twice that of the square specimen at the final IP pre-damage level. Moreover, the squat wall shows a more drastic drop in OOP strength, with the majority of it happening in the low damage levels (<0.4 % IP drift), suggesting that the critical value of the IP pre-damage drift reduces in walls with low aspect ratios [101]. This is because such walls are more prone to localized damages during IP testing due to the formation of diagonal struts within the specimen. The diagonal struts cause larger stress concentration at the corner of the specimens, which leads to more pronounced crushing and loss of composite action with the frame [39,116]. This, in turn, creates residual OOP deflections and increases the degradation of OOP performance [44]. The other 2 walls tested during the campaign have higher thicknesses (h/t = 15.2) and different aspect ratios (l/h=1.3 and 1.0). Also in this case, a similar, faster degradation of the OOP response is observed in the squat wall; yet, the final drops in strength and stiffness are similar to those of the square wall. This observation, along with the low sensitivity of the less slender walls numerically studied in [43], suggests that thicker walls are less sensitive to the variations in aspect ratio as well as IP/OOP interaction effects.

4.1.3. *Masonry material properties*

The categorization of experimental and numerical specimens based on the type and strength of masonry materials used in their panels, as well as the classification of experimental specimens based on the type of mortar, is presented in Fig. 9.

Different configurations and material compositions are used following various construction techniques adopted in practice. For what regards the masonry units in the infill walls, clay units are used for 86 % of specimens, while 9 specimens are made of concrete blocks in [43,71,72,88,89] (see Fig. 9.A.1). Among the former, only the 18 walls tested in [27,71,75,77,86,87,96] are made with solid clay blocks, while the remaining 38 specimens adopt perforated blocks with holes laying in a vertical or horizontal direction to represent local construction practices. Specifically, 31 specimens have horizontal holes [73,74,76,83,84,90–92,95,98,99,101,103,104], whereas in the remaining 7 walls, the holes are aligned in the vertical direction [78,80–82,93,94,109]. The concrete blocks used in the tested walls are all perforated, and the holes are oriented vertically [71,72,88,89]. Regarding the different types of mortar used during the experimental campaigns, 85 % of the specimens are assembled using a cement-based mortar with the common-purpose 1:1:6 (cement:lime:sand) mixture, while a 1:3:12 mortar is used for 6 specimens [84,85]. Additionally, 3 specimens in [37] are constructed with a weak lime-based 1:3 (lime:sand) mortar to investigate specifically the effect of such material variation. Concerning the finishing of the head joints, the typical configuration (80 % of the tested specimens) involves filling them with mortar. However, in the 13 specimens tested in [78,80,81,93,94,99], the head joints are left dry, and the masonry units in each row are interlocked by means of tongues and grooves. The masonry unit types and mortar compositions listed for the numerical studies (see Table 2) represent the properties of the tests that are used to calibrate the numerical models, especially for those using the macro-element approach [13,41,42], rather than specific simulation assumptions.

The type and the layout of the masonry units directly affect the compressive strength and other mechanical properties of the masonry panels. This is apparent in Fig. 9.C, where the vertical compressive strength of experimentally tested and numerically simulated masonry assemblies (wallets) is shown, grouped based on the different masonry unit types. Perforated clay blocks exhibit the lowest compressive strengths in the case of horizontal holes (<4 MPa), whereas higher values are measured in the case of vertical holes (3–6 MPa). Even higher values are obtained for solid clay bricks (6–10 MPa). Regarding the concrete blocks, only a few scattered data points are available for vertically-perforated concrete blocks. In general, the compressive strength of such blocks is significantly higher (9–22 MPa) than that of

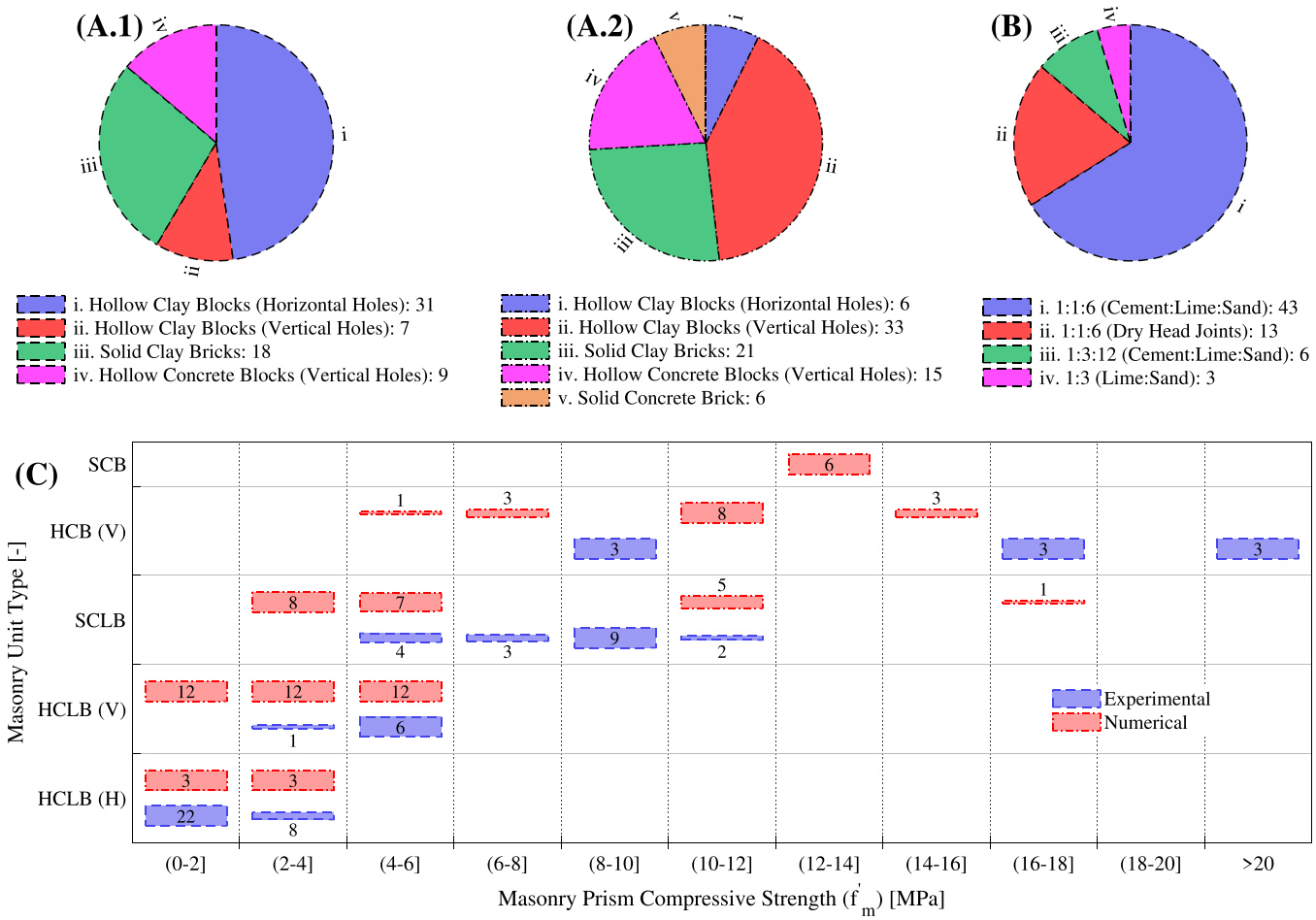

Fig. 9. Variations of mechanical properties explored in experimental and numerical studies of IP/OOP interaction effects in framed URM walls: type of masonry units adopted in experimental (A.1) and numerical (A.2) specimens, mortar types used in experimental specimens (B), and the range of masonry prism compressive strength in experimental and numerical specimens (C). For the meaning of abbreviations, please refer to the Nomenclature.

the corresponding clay blocks. In case of horizontally-perforated concrete blocks, no experimental characterization is available, while 6 walls are studied numerically [51] assigning a compressive strength similar to that of high-strength solid clay brick panels (10–12 MPa). It should be noted that compressive strengths reported herein refer to the masonry and not to the units, and are based on the unit orientation as used in wall construction. For perforated blocks laid with vertical holes, the compression strength of wallets parallel to the holes is considered; for perforated blocks laid with horizontal holes, the strength ow wallets perpendicular to the holes is used.

Different compressive strength of masonry influences the wall performance, as the occurrence of crushing failure, caused by stress localization in the diagonal struts or by arching mechanisms, largely depends on this parameter [73]. Moreover, local failures of a portion of masonry units, more likely in the case of perforated low-strength blocks, may occur depending on the distribution of pre-damage [80].

Experimental data primarily focus on low-strength masonry materials ($f'_m \leq 6$ MPa), a wide range of compressive strength values is considered. Moreover, a detailed investigation of the influence of compressive strength on the IP/OOP interaction effects cannot be conducted because almost no campaign varies consistently with this parameter, so its effects are combined with those of geometrical and loading conditions. Only 2 specimens in the tests conducted by [71] are built with similar geometry (l/h=1.5, h/t = 16.5 and 17.7) but different materials: 1 with vertically perforated concrete blocks (f'_m=22 MPa) and the other 1 with solid clay blocks (f'_m=7.4 MPa). However, the capacity of the loading apparatus is reached before the walls reach OOP failure. At the end of the test, both specimens exhibit diagonal cracks that propagate from their middle region to the corners, with no compressive failure, and thus do not provide useful indications on the relevance of masonry compressive strength to wall performance.

A numerical sensitivity analysis is conducted in [43] to investigate the interaction effects in vertically perforated concrete block walls with different geometries and material properties. Specifically, three classes of blocks are adopted, representing a weak (f'_m=8 MPa), intermediate (f'_m=12 MPa), and strong (f'_m=16 MPa) material. The elastic stiffness and tensile strength of each class are also varied proportionally to the compressive strength. It is observed that, while the interaction effects under light IP pre-damage (IP drift < 0.25 %) are similar in all walls, the panels with intermediate material exhibit the least degradation of the OOP response under higher IP pre-damage. This is achieved through improved crack propagation to the wall during IP loading. Strong infill walls exhibit the development of a diagonal crack, characterized by both tensile cracking and crushing of the blocks, along with increased damage in the surrounding frame due to the formation of geometrically larger diagonal struts during IP loading. In infill walls with weak blocks, shear cracks develop during IP loading along the bed and head joints, leaving crack paths that are easily re-opened during OOP loading. This is, however, less critical than in the case of strong masonry, due to the reduced damage in the surrounding frame and the blocks in the panels. Both the IP mechanisms (development of diagonal struts and shear cracks) are minimized in infills with intermediate material properties, so that lower strength and stiffness degradation is obtained in the OOP direction. It is important to note that the extent of the influence of the

material properties varies depending on the geometry of the walls. Namely, the differences are more pronounced in the case of walls with high aspect and slenderness ratios, while they decrease for less slender and square walls.

The numerical parametric study in [13] on square walls (l/h=1.0) with different slenderness ratios (h/t = 26, 13, and 8.6), considers varying compressive strengths of masonry units, assuming them as perforated clay blocks with vertical holes with a range of strength (1–6 MPa) lower than those considered by [43]. It is observed that high-strength materials (f'_m=6 MPa) lead to lower sensitivity of OOP strength and stiffness to IP pre-damage, especially in thicker specimens (h/t ≤ 13). The thickest wall (h/t = 8.6) with strong material (f'_m=1 MPa) shows a 40 % lower strength drop at 1 % IP pre-damage drift and 60 % lower stiffness drop at 0.5 % IP pre-damage drift compared to the one with weak properties. Although a macro-element model is used in the study and no description of differences between the damage mechanisms of weak and strong specimens is given, it is believed that the larger sensitivity of weak walls is due to the occurrence of crushing during IP loading, which does not occur in stronger specimens. The lower sensitivity of the thinnest walls (h/t = 26) to material properties supports the aforementioned conclusions, as these specimens experience lower compressive stresses due to reduced vertical confinement effects and, consequently, exhibit lower crushing across different material variations. It should also be noted that all specimens reach similar amounts of OOP stiffness reduction under an ultimate 2 % IP pre-damage drift level, with stronger specimens showing only as much as 20 % higher OOP capacity compared to weaker ones. Another interesting observation is that the walls with low compressive strength (1–3 MPa) show very similar sensitivities to IP/OOP interaction effects across all slenderness ratios, denoting that extremely low strength in masonry panels may lead to severe influence of IP pre-damage on OOP response regardless of the geometrical configuration of the walls.

The interaction effects are shown in [71] to also be influenced by the mortar composition, as specimens with stronger cement-based mortar exhibit higher OOP strength reduction at the same IP pre-damage level compared to those constructed with lime-based mortar, especially in the case of high slenderness ratios. The larger strength reduction in the case of stronger mortar is caused by the sharp localization of the cracks, which leads to overlapping cracking paths of IP and OOP responses. In contrast, cracks are more spread throughout the panel in the case of the lime-mortar specimens.

4.1.4. Surrounding frame material

Regarding the material used for the frames, 97 % of experiments focus on panels with RC frames, and Steel frames are used only in 2 specimens [73,103]. Steel frame is also used in the 3 experiments of [102], but together with concrete to replicate the effect of strong-beam/weak-column mechanism observed in non-seismic RC frames. Differences are reported in the case of unidirectional OOP loading: Steel frames have more ductility and lower strength compared to RC frames, as well as weaker bond with the masonry panels [88,89,117], hence, increasing the IP/OOP interaction effects. However, the lack of sufficient experimental and numerical studies impedes the conclusive comparison of the influence of frame material on the behavior under interaction effects.

The effect of the strength of RC frames on IP/OOP interaction effects has only been the focus of [75] and [77], testing 2 IM walls, one within a weak frame and the other in a stronger frame. However, the results of these two tests are not comparable due to the differences in the geometrical properties of the specimens, specifically their height-to-thickness slenderness ratio. A numerical investigation in [45] simulates 2 RC frame walls with similar geometrical and material properties (l/h=0.9, h/t = 12, and f'_m=3 MPa) one placed in a strong frame, and the other surrounded by a weaker frame with 40 % smaller column cross-sections. The specimen with a stronger frame shows a 10 % higher OOP strength reduction at different IP pre-damage levels compared to the weaker-frame wall. This is because, although the damaged OOP strengths and stiffnesses are similar between the masonry panels of the two, the strong-frame model has a higher pristine OOP strength. This implies that, despite the slight differences in OOP strength resulting from having a stronger frame, the effect of frame strength on OOP response dissipates and becomes insignificant compared to the frame/panel connection upon taking the slightest IP damage.

4.1.5. Loading protocol and boundary conditions

The categorization of the available experimental and numerical data based on their variations in IP/OOP interaction scenario, as well as boundary conditions, loading procedures, and loading apparatus, and the initial vertical load adopted for IP and OOP loadings is presented in this section and illustrated in Fig. 13.

4.1.5.1. IP/OOP interaction scenario. According to Fig. 13.A, 74 % of experimental specimens studied for IP/OOP interaction effects are tested under SQ, 20 % under SC loading, 5 % under CB pre-loading [71–73], and 1 % under SM loading [90]. For the 13 specimens under SC loading, 12 tests [27,75,77,86,87,96] start with OOP loading. The OOP loading steps of these tests are all performed with the same load magnitude, while the IP loading is increased at each subsequent step. The remaining 1 SC test [93] starts with IP loading, then one step of OOP loading, and then another final step of IP loading. Similarly, 82 % of numerical simulations adopt SQ loading, and only 7 % [51] an 11 % [42] are performed via CB and SM loading, respectively.

Only 2 experimental campaigns allow for a comparison of the wall performance under SQ and CB loading. Two couples of similar walls are tested in [73] following either a SQ or a CB protocol. To facilitate comparison, the value of the IP pre-load in the SC tests is kept the same as the maximum IP load applied to cause pre-damage in the SQ tests. Slight differences are observed between the OOP responses under the different loading scenarios, also due to the limited capacity of the testing apparatus which prevents the specimens from reaching failure. The most remarkable difference is that the walls subjected to CB loading show an increase in the initial OOP stiffness due to the confinement of the panels in one diagonal direction determined by the pre-loading. However, this is followed by a steeper reduction in OOP stiffness compared to the SQ wall after the confinement effects decrease. In the campaign conducted by [73], the IP load applied for the SQ and CB tests is different, making a direct comparison of the two tests difficult. Nevertheless, it is reported that the presence of IP pre-load in the case of CB protocol fosters an overall stiffer behavior during OOP loading, but also results in 30 % lower strength due to increased crushing.

Considerations regarding the interaction effects in the case of SC and SM are derived from the comparison of the dynamic tests conducted by [75] and [90], the results of which are shown in Fig. 10. In the former campaign [77], an unusual SC loading sequence is considered. First dynamic OOP loading is applied incrementally up to a PGA of 0.4g. Then, a new loading sequence for which quasi-static cyclic IP loading of increasing intensity is alternated with OOP dynamic loading with a fixed 0.4g intensity is adopted. The test continues until the collapse of the top portion of the wall during the OOP test conducted after completing an IP run with a cyclic amplitude equal to 2.2 % drift. In the latter [90], 5 SM tests are conducted with bi-directional dynamic loading, based on tectonic earthquakes. The load intensities are gradually increased in each step up to 0.63g and 0.79g in the IP and OOP directions, respectively. It should be noted that the proportionality of the IP and OOP loading signals is not kept constant in different steps of the SM test. Both SC and SM walls show similar crack patterns with several major horizontal cracks forming at different elevations, as well as diagonal cracks extending from the center of the panels to their base. However, in the case of the SM protocol, more pronounced interaction effects are observed, leading to a 90 % reduction in OOP stiffness and a 950 %

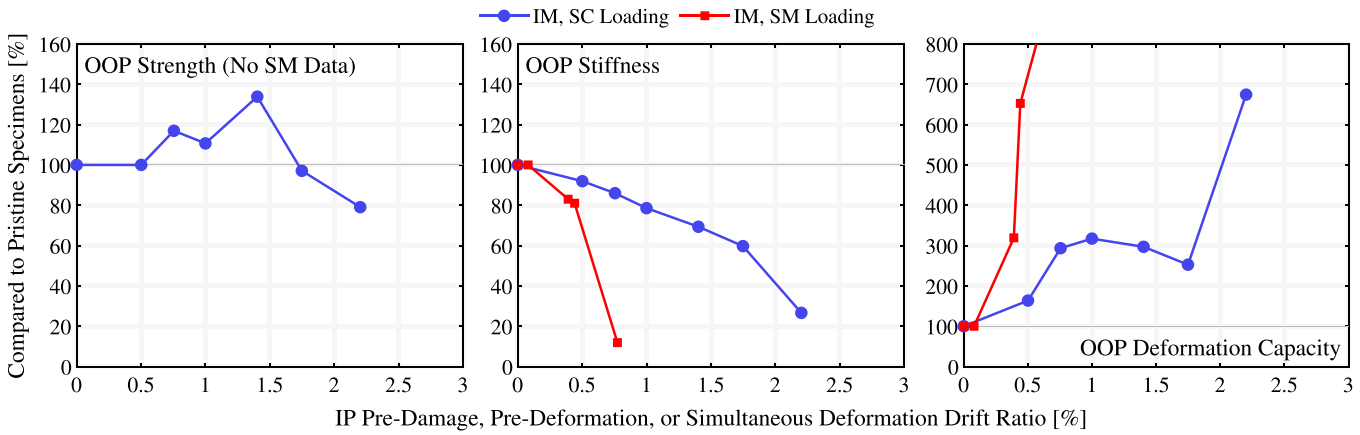

Fig. 10. Example results of IP/OOP interaction effects in walls tested under different interaction scenarios. The data are extracted from [75,90]. For the meaning of abbreviations, please refer to the Nomenclature.

increase in OOP deflection during the final step of the experiment, when a maximum 1 % IP drift is recorded. In contrast, the SC wall experiences only a 20 % OOP stiffness drop and a 220 % OOP deformation increase at 1 % IP pre-damage drift, and achieves a 75 % stiffness drop and a 575 % OOP deformation increase only after a 2.2 % IP pre-damage drift is applied. Although different materials are used (lower-strength hollow clay blocks with horizontal holes are used in the SM tests, and solid clay blocks are used in the CB tests), consistent trends regarding the influence of IP/OOP interaction are observed from the start of the experiment. For this reason, it can be concluded that higher IP/OOP interaction is expected in a simultaneous IP and OOP loading scenario.

4.1.5.2. IP and OOP boundary conditions. The choice of boundary conditions directly affects the development of alternative IP and OOP failure mechanisms and cracking patterns of the walls, which in turn leads to different IP/OOP interaction effects [18]. The IP load is applied to all the experimental and numerical simulations in a double-clamped setting, where the top beam of the frame is restricted from rotation around the OOP axis to favor a shear-like response of the wall. Moreover, all of the OOP loading steps of the tests and simulations are done in a two-way spanning OOP configuration to best represent the behavior of real-world framed walls. Only in the 2 experiments of [74], one-way spanning boundary conditions are applied in OOP. In these cases, the OOP load is applied at the mid-height of the walls [74] while the OOP movement of the top beam is restrained to form a pinned one-way bending mechanism. In all specimens, a full connection is established between the panel and the frame, allowing the composite action of the two structural elements during IP loading, as well as the development of a two-way arching mechanism during OOP loading. Any substantial gap between the frame and panel that develops during the IP loading phase reduces the OOP strength and stiffness, as well as increases the OOP deformation, due to the change in boundary conditions [73,80,93,98,118]. This is also important for real-world assessments, as long-term creep and deformation of frames and/or panels may lead to the formation of discontinuities between walls and frames, which may in turn reduce OOP resistance [119,120].

A concrete conclusion cannot be reached regarding the effects of OOP boundary conditions due to the limited available data. Nevertheless, a brief comparison of the observations from the tests [74] on the behavior of 2 one-way bending walls (l/h=1.5 and h/t = 23.9) under frame drift OOP loading with those from [91] on 3 similar walls (l/h=1.3 and h/t = 22.8) under Wall Face Five-Point Loading (WF5PL) two-way bending OOP loading is presented. While all pre-damaged by applying cyclic IP loading in double-clamped configuration, the one-way bending walls exhibit a 20 % larger OOP strength drop but a 40 % lower stiffness reduction compared to the two-way bending walls, respectively, at a moderate pre-damage level (0.4 % IP drift). Moreover, the one-way bending walls maintain stability until a pre-damage level twice as large as the two-way bending walls (corresponding to 1.2 % IP drift in the former compared to 0.6 % in the latter). Although [74] does not provide the final crack pattern of the one-way bending walls, it is suspected that the lower sensitivity of one-way bending walls to IP pre-damage is because their OOP cracking mechanism does not coincide with IP crack patterns as much as two-way bending walls [18]. In other words, while during OOP loading, damaged two-way bending walls show the re-opening of most of the same cracks already appeared during IP loading, the one-way bending OOP mechanism involved primarily the horizontal cracking of the mid-height of the wall, which is as affected as much by double-clamped IP step cracks.

4.1.5.3. Loading procedures. Different loading procedures for IP loading have been selected by researchers. The choice depends primarily on the research objectives, but also on specific technical restraints, such as costs and availability of proper facilities [121]. According to Fig. 13.B, The IP load is applied by imposing a quasi-static cyclic (QSC) or monotonic (QSM) load to the top beam of the specimen in 89 % of the experiments as well as 70 % of numerical simulations. The QSM loading is used in the 6 tests of [43,88,89]. Only in the 1 test conducted by [90], dynamic IP load is applied via a shake table (ST). For those experiments conducted via cyclic loading, the loading sequence consists of a series of cycles targeting specific drift levels and progressively increased in magnitude. Fig. 13.C shows that OOP load is also applied in quasi-static conditions for 75 % of the tests. In detail, 57 % of the tests use QSM loading and 17 % [73,80,84,98,104] use unidirectional load-unload cycles (QSLUC). The latter are characterized by the application of half cycles. In other words, the load is applied up to a certain level, followed by full unloading, and when the specimen has returned to the zero-load condition a new loading cycle (either of equal or of increased intensity compared to the previous cycle) in the same loading direction. Such procedure allows testing the wall under cyclic loading while having access to one side of the panel for tracking the failure patterns [2]. Fully QSC loading (for which cycles of equal amplitude are applied in both the positive and negative loading direction) is adopted only in the numerical study of [42] where such practical concerns are irrelevant. Additionally, dynamic seismic accelerograms are applied via shake table motions for only 16 tests conducted in [27,75,77,86,96,102]. Finally, 1 experiment [100] analyzes ambient vibrations [122–124] to identify the changes in OOP stiffness after IP pre-damage. All in all, the lack of tests applying QSC loading in the OOP direction and of experiments applying IP pre-damage determined by dynamic loading.

No comparative experimental campaign has been conducted to determine the sensitivity of interaction effects to different IP loading

procedures. However, a numerical investigation in [43] compares the differences in the interaction effects for IP pre-damage obtained via either QSC or QSM loading, showing that the OOP capacity of walls with different aspect ratios undergoes up to 13 % higher reduction when IP pre-damage is applied through QSC loading, especially for moderate pre-damage levels. However, both the resisting mechanisms and the final crack pattern are similar under both loading procedures. For these reasons, the sensitivity of the interaction effects to this specific aspect can be considered moderate to low. It should be noted that a numerical campaign has recently been initiated to investigate the suitability of different loading protocols for studying interlocking masonry IM walls subjected to unidirectional IP and OOP loads, as well as their interaction effects [121].

The sensitivity of the interaction effects to different OOP loading procedure is discussed by comparing different experimental campaigns that studied comparable walls, i.e. the data shown in Fig. 11. In [99] and [80], QSM and QSLUC tests are conducted, respectively, by applying four-point OOP load on two specimens having similar aspect ratios (l/h of 1.6 and 1.4, respectively) and slenderness ratios (h/t of 8.8 and 8.4, respectively). While both tests show similar OOP strength reduction, the increase in the maximum OOP deformation of the QSLUC specimen is 200 % more than that of the QSM wall despite the use of stronger materials. Moreover, significant differences in the OOP damage patterns are recorded, with the cracks being distributed to the whole QSM wall, while more localized damage and wide cracks close to the mid-height of the wall are observed in the QSLUC specimen. It should be noted that the loading points of the QSLUC test are located closer to the mid-height of the wall and are not as spread-out as the those in the QSLUC test, which may partially justify the differences highlighted above. Moreover, the stronger vertically laid perforated blocks used by [80] might have caused the lower inelastic deformation of the blocks and concentration of damage in the mortar [71]. Nevertheless, the QSLUC and QSM airbag tests conducted in [93] on walls with identical material and geometry (f'_m=3.1 MPa, l/h=1.1, and h/t = 6.9) show similar differences in damage patterns, with more pronounced crack localization at the four edges of the QSLUC wall. Finally, a comparison between the QSLUC airbag test conducted in [84] (l/h=1.8 and h/t = 15.3) and the QSM experiment of [71] (l/h=1.5 and h/t = 16.5) further confirms the difference of outcomes obtained for cyclic and monotonic loading, with more evident crack localization in the case of QSLUC and major cracks at top and side frame/wall interfaces. It is therefore concluded that cyclic loading promotes crack localization, resulting in lower damage diffusion.

The last comparison focuses on tests for which the OOP loading is applied via airbags in QSLUC or dynamically via a shake table (ST). The comparison between the tests reported in [98] and [75] on walls with similar geometries (l/h=1.5 and h/t = 19 in the former and l/h=1.7 and h/t = 22.8 in the latter), reveals different OOP performances. The first wall, tested in QSLUC conditions, experiences a more drastic degradation in OOP performance at low IP pre-damage drifts (0.5 %) compared to the ST-loaded wall, although this may be attributed to the use of lower-strength masonry units (see 4.1.3). However, the ST wall exhibits a more brittle behavior at subsequent stages, with the development of localized cracks at the side and bottom frame/panel interfaces, as well as one diagonal crack connecting the bottom left and top right corners of the wall. Contradictory observations are obtained from the numerical study in [51], which considered walls with identical geometry and materials and different OOP loading procedures. The outcomes of the analyses do not show any different OOP stiffness and strength degradation for QSLUC walls compared to ST walls. It should be noted that the QSLUC-tested wall of [98] has been conceived as a cavity wall, formed by two slender leaves, which may have resulted in its higher sensitivity to IP/OOP interaction effects. In conclusion, the limited data available does not allow for any decisive conclusion regarding the sensitivity of interaction effects to the application of quasi-static or dynamic OOP loading.

4.1.5.4. Loading apparatus. The instruments by which OOP loading is applied to the walls affect the damage pattern as well as the wall capacity [117]. The variations considered for the OOP loading instruments of tests and the related number of specimens are shown in Fig. 13.D. In the case of the 16 dynamic tests [27,75,77,86,90,96,102], ST is used. Quasi-static experiments, on the other hand, employ a variety of loading apparatus and methodologies. The first distinction involves the application of quasi-static load to either the surrounding frame (FD) or the masonry panels directly. The FD is adopted for 2 quasi-static tests [74], but it is shown to concentrate the damage to the frame elements rather than the masonry wall [17]. Hence, the direct loading of the panels is used in the majority of the reported quasi-static experiments (96 %). The OOP load is applied to the surface of the masonry panel via two alternative types of loading apparatus. The first option consists of the imposition of OOP displacements at multiple points on the surface of the wall (WFMPL), and is used to apply OOP load at four points (WF4PL) in 12 experiments [75,77,81,96] and at five points (WF5PL) in 11 tests [87,88,92,97]. The second option ensures a virtually uniform distribution of OOP pressure to one or both sides of the walls via airbags (AB) and is used in the remaining 23 tests [43,71,73,76,84,88,89,93,98]. Finally, 1 experiment [100] adopts a non-destructive OOP testing approach, where ambient vibration identification is used to measure the effect of IP pre-damage on natural OOP frequencies of the specimen from its accelerations under environmental excitation, such as due to the passing of vehicles or lab workers. In the numerical simulations, AB lading is used

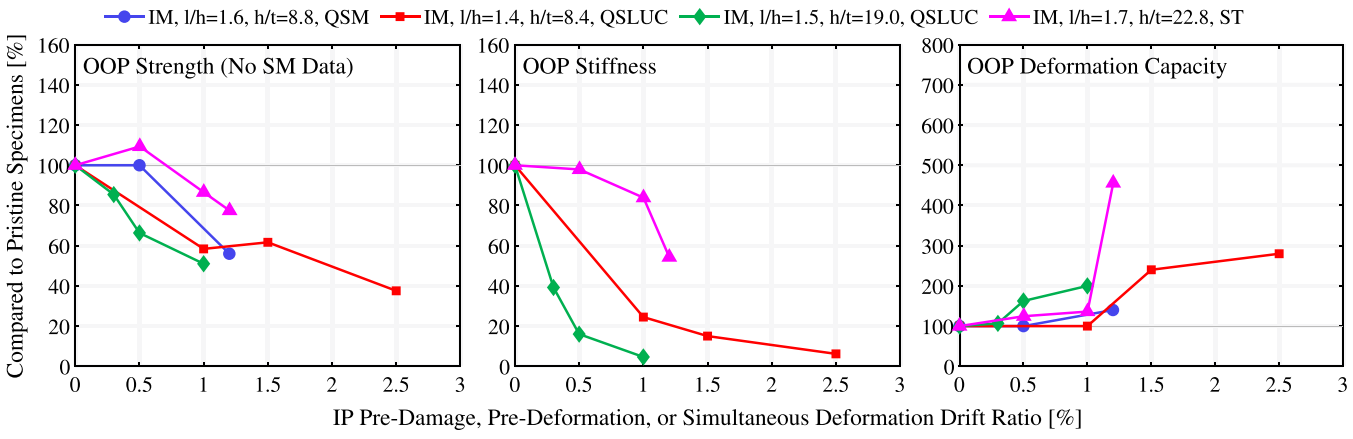

Fig. 11. Example results of IP/OOP interaction effects in walls tested under different OOP loading protocols. The data are extracted from [75,80,98,99]. For the meaning of abbreviations, please refer to the Nomenclature.

in 47 % of the cases. However, 50 % of simulations use a point load at the mid-center of the panels (referred to as WFMiPL and categorized in Wall Face Multi-Point Load in Fig. 13.D). This is because, although calibrated against experiments under AB loading in OOP, these simulations [13,41,42] are done via macro-element models wherein only WFMiPL is possible.

Typically, each experimental campaign utilizes a single type of loading apparatus, and hence, no direct comparison is possible between the consequences of selecting one procedure over another. However, [98] and [91] have 2 tests on walls with similar geometries and material properties (f'_m=1.2 MPa, l/h=1.5, h/t = 19 in the former, and, f'_m=1.8 MPa, l/h=1.3, and h/t = 22.8 in the latter) for which the OOP load is applied via AB and WF5PL, respectively. According to the results shown in Fig. 12, the AB wall exhibits a similar damage progression to the WF5PLone, with most of the cracking and OOP response degradation occurring at low IP pre-damage level (0.5 % IP drift). The two walls also experience similar ultimate OOP strength and stiffness drops at 1 % IP pre-damage drifts. However, the WF5PL wall exhibits almost half the increase in OOP deformation, with damage more localized around the load application points, in the form of crushed and fractured masonry units. Conversely, the airbag wall shows a more diffused damage pattern with stepped cracks along the mortar joints and detachments at the frame/panel interfaces, which is close to the failure mode observed in testing of a wall with similar geometry under closer-to-reality ST load [75]. Consequently, the AB loading could be considered to better mobilize all parts of the specimens and provide a more accurate representation of OOP seismic loading, for which all regions of the walls are excited by inertial forces.

4.1.5.5. Initial vertical load. The presence of an initial vertical load may also affect the performance of the tested infill walls, as it contributes to the confinement of the wall during IP loading and the development of vertical arching effect during OOP deformation [51]. As shown in Fig. 13.E, 70 % of experiments [27,74–78,80,83,90,93,94,96,98,99,125] apply a vertical pre-compression load before the start of the loading in IP or OOP directions to simulate the behavior of the specimen as part of a multi-story building. However, different solutions have been selected to apply the load. In 33 cases [74,76,78,80,83,90,93,94,98,99], the tests are conducted with pre-compression applied only to the RC frame columns. For those, the magnitude of the vertical load covers a comprehensive range, varying between 4.4 % and 40 % of the compressive axial strength of the columns. Regarding the numerical simulations, 57 % of the instances are done without considering vertical load, 38 % [41,42,45,89] consider column load between 1 % and 25 % of the column axial capacity, and only 5 % [51] include a minor additional load on the walls, as much as 5.2 % of the masonry compressive strength (f'_m).

The assessment of the effects of pre-compression on the IP/OOP interaction is limited to a few experimental campaigns. In [71], no relevant difference with the inclusion of vertical load is reported, while [85] reports some limited effects. In this latter case, a small column vertical load (4.4 % of the column axial capacity) determines a limited improvement of the OOP load-bearing capacity, because only 7 % of the column load is transferred to the masonry panel [71]. On the other hand, [98] show that high pre-compression levels (40 % of the column axial capacity) can increase the OOP strength and stiffness by 50 % under a specific IP pre-damage, as well as decrease the rate of OOP strength reduction for increasing levels of pre-damage.

Regarding the application vertical load on the walls, the 12 tests conducted during the campaign reported by Singhal and Rai [27,75,77,86,96] include a limited vertical load on the top beam (1.5 % of the compressive strength of the masonry assembly) in addition to the application of axial load to the columns. However, the consequence of this additional load is not discussed in the paper, as the authors assume it to have a minor effect on the IP/OOP interaction. On the contrary, the numerical study conducted by [51] highlights the sensitivity of the interaction effects to the presence of a vertical wall load. Specifically, applying a load equal to 5.2 % of the compressive capacity of the masonry panel to the concrete beam significantly delayed the interaction effects, resulting in an IP pre-deformation two to three times larger than the corresponding case without a vertical load. Such improved performance could be attributed to the increased deformation and strength capacity of the wall in the IP direction, which results in the postponement of IP damage and subsequent OOP response degradation to larger drifts [51].

4.2. Effects of OOP response on IP wall behavior (OOP/IP interaction)

As introduced at the beginning of 3, only 4 experimental campaigns [73,93,103,104] have been conducted to investigate the influence of OOP pre-damage and pre-load on the IP response of framed masonry walls, yielding only the 10 data points illustrated in Fig. 14 and making it impossible to discuss the OOP/IP interaction effects at the same level of detail as for the IP/OOP interaction effects. For this reason, a more comprehensive discussion, encompassing both experimental and numerical findings, is presented herein. Specifically, 6 walls are tested experimentally, and the structural response of 36 specimens, including 14 walls [5,16,38,40] and 22 multi-bay multi-story frames [5,28,32], is simulated numerically. Both experimental tests and numerical simulations of walls primarily consider sequential and combined loading scenarios for the application of OOP and IP load: 5 walls are tested under SQ and 1 wall [93] under CB loading. Moreover, 13 out of 14 numerical wall

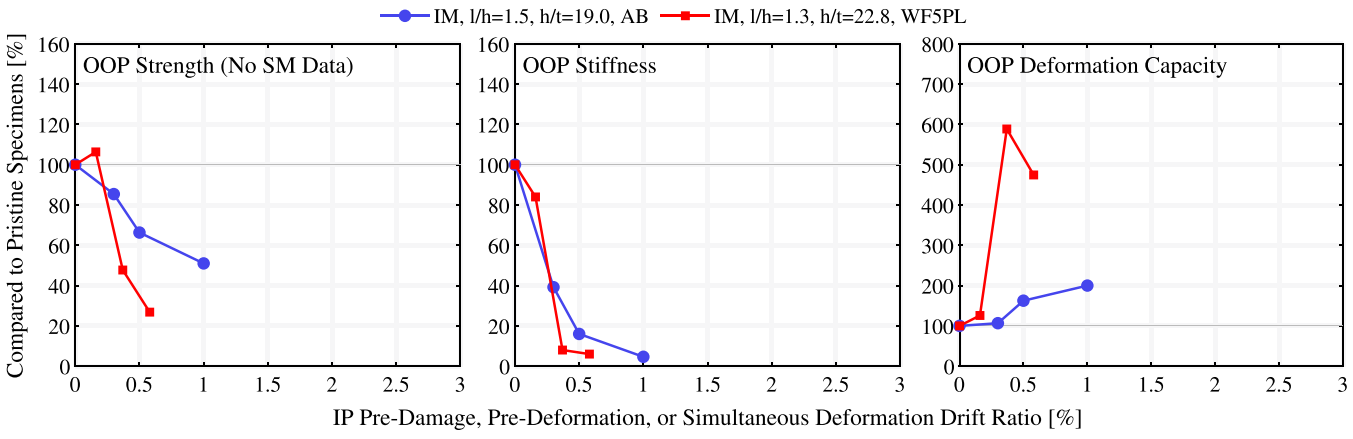

Fig. 12. Example results of IP/OOP interaction effects in walls tested under different OOP loading apparatus. The data are extracted from [91,98]. For the meaning of abbreviations, please refer to the Nomenclature.

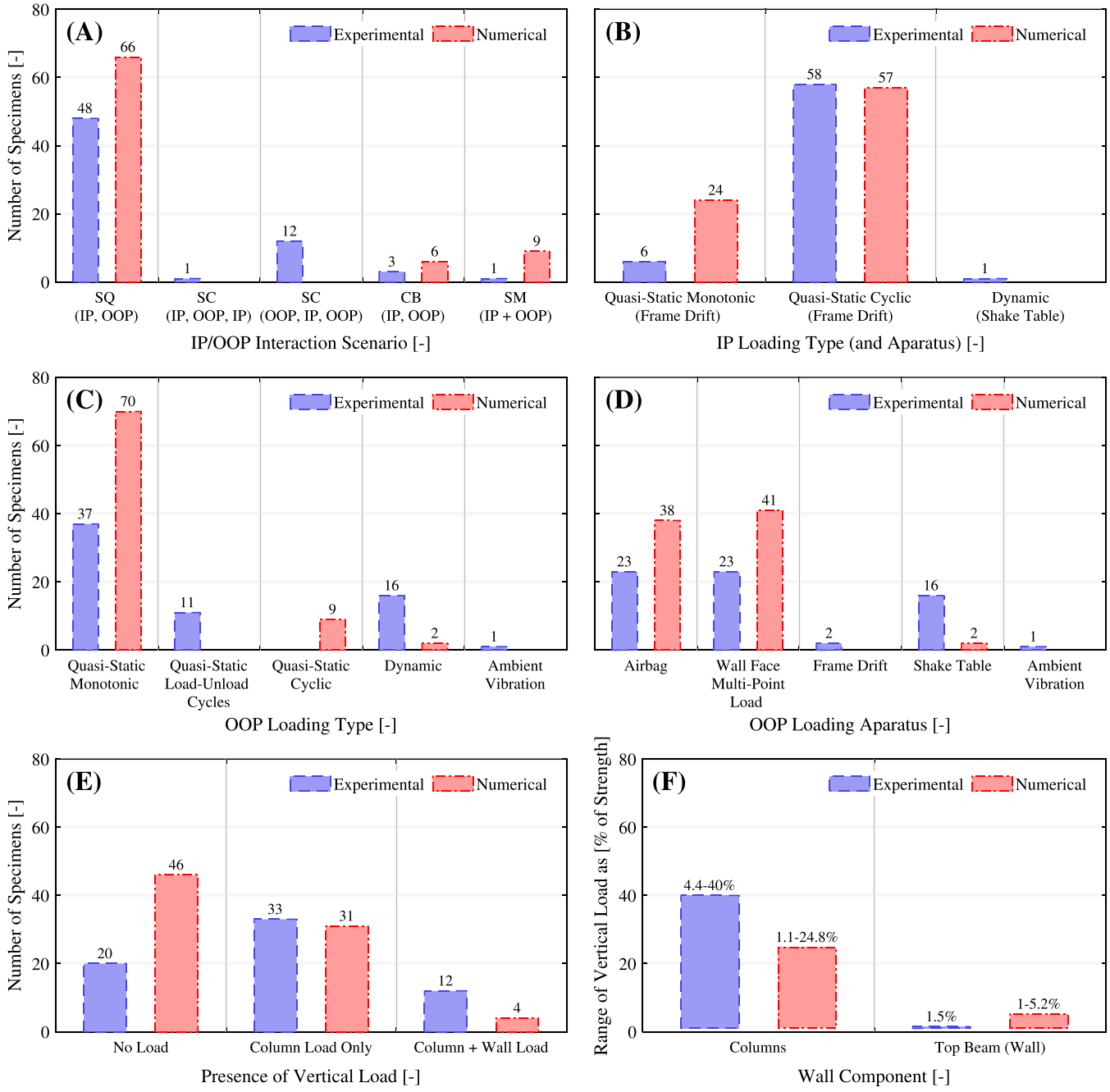

Fig. 13. Loading assumptions explored in experimental and numerical studies of IP/OOP interaction effects in framed URM walls: interaction scenario (A), in-plane loading type (B), out-of-plane loading type (C) and apparatus (D), and presence (E) and range of magnitudes (F) of initial vertical load. For the meaning of abbreviations, please refer to the Nomenclature.

simulations consider CB loading, while SM application of OOP and IP load is used for the remaining 1 wall in [30] and all 22 frame analyses. It is noteworthy that OOP pre-load and pre-damage, respectively used in SQ and CB loading scenarios, are conservatively applied below the OOP peak capacity of the specimens. This is because the walls are expected to lose the integrity and resistance required for a subsequent IP loading after they exceed their OOP strength. In the next sections, the OOP/IP interaction effects reported in the literature are discussed based on the adopted loadings scenarios.

4.2.1. OOP pre-damage (sequential loading)

The experimental outcomes of SQ tests in [73,103,104] show that the effect of OOP pre-damage on IP response is not as significant as the influence of IP behavior on OOP performance, yet not always negligible. In the 1 SQ experiment in [73] conducted on a thick square wall (l/h=1.0 and h/t = 11.2) assembled with hollow clay blocks laid in horizontal arrangement, the specimen is loaded first in OOP two-way bending via airbag and then in IP in a double clamped configuration. Although pre-damaged up to 70 % of its OOP capacity, the specimen shows the same IP performance in terms of strength, stiffness, and deformability as the reference purely IP-loaded specimen. Higher sensitivity is observed in the 1 test conducted in [104] on a squat thin wall (l/h=1.3 and h/t = 25.9) with similar material properties and boundary conditions to those of the thick wall of [73]; the specimen, OOP pre-damaged via Wall Face Six-Point (WF6PL) two-way bending loading of the panel surface, shows 25 % strength drop and 47 %

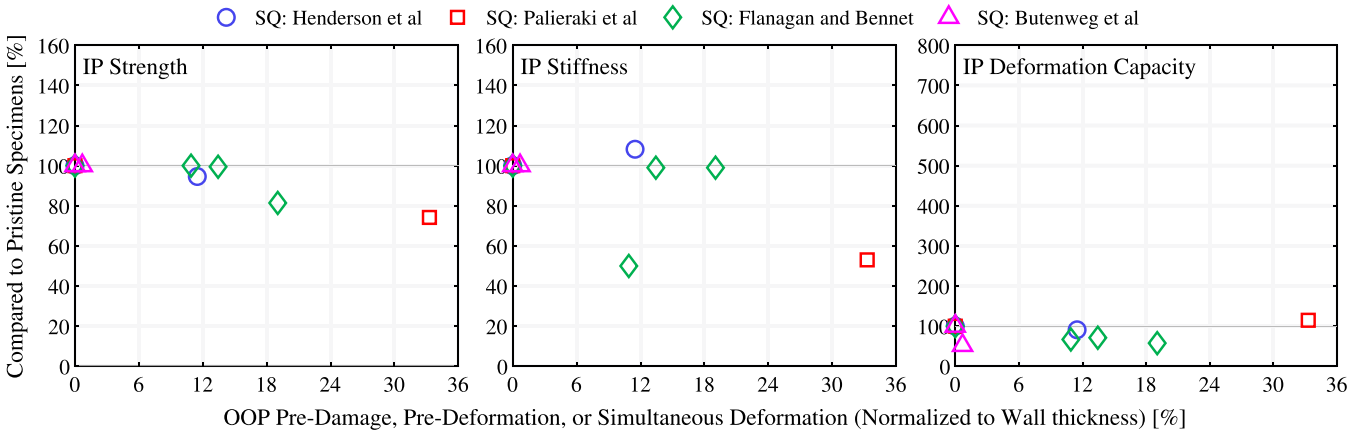

Fig. 14. Overview of data points collected from the outcomes of experimental investigations on the effects of OOP/IP interaction on IP behavior of framed URM walls [73,93,103,104]. For the meaning of abbreviations, please refer to the Nomenclature.

stiffness reduction during the IP double-clamped loading. However, such changes are observed under OOP pre-damage levels that are 150 % higher than those considered for the thick walls (corresponding to OOP deformation up to 33 % of wall thickness). It is observed that the diagonal cracking that develops during double-clamped IP failure follows a separate path from the one that forms at light OOP two-way bending pre-damage. Hence, under low to moderate OOP pre-damage, the IP behavior remains similar to that of a virgin specimen. On the contrary, in the case of severe OOP pre-damage, the development of diagonal cracking similar to that at IP failure can lead to noticeable degradation of the IP performance. In case of one-way bending cantilever boundary conditions considered for 2 walls tested in [73], the application of OOP pre-damage via a top drift equal to 19 % of the wall thickness reduces the IP strength by approximately 20 % by causing bed-joint cracks at the base of the wall that re-open during IP loading.

4.2.2. *OOP pre-load (combined loading)*

Walls under CB loading show higher OOP/IP interaction effects in the presence of OOP pre-load compared to SQ cases [16]. The only available CB test [93] on 1 wall (l/h=1.1, h/t = 6.9) shows that OOP two-way bending deformation caused by pre-load can prevent the full development of the wall double-clamped IP load-bearing capacity and instigates brittle failure at significantly lower IP drifts compared to virgin walls without OOP Pre-load. In fact, an OOP airbag pre-load as much as 20 % of the OOP capacity, alters the damage progression and even change the failure mode of the wall during IP loading: tensile and compressive failure of the bricks at the base of the wall is observed instead of pure diagonal cracking during the IP loading step in the CB experiment.

The 13 numerical CB simulations [5,16,38] are done for single-story single-bay reinforced concrete frames infilled with solid clay brick walls, assembled in single-wythe. Quasi-static monotonic IP frame drift and OOP airbag pre-loading with double-clamped and two-way bending boundary conditions, respectively, are adopted in the simulations. Only the 8 [38] conducted via a macro-element model adopt WMiPL loading in OOP due to technical limitations. Similar material properties are considered for all specimens, with the masonry panels having compressive strengths in the range of 1–4 MPa and common-purpose cement-based 1:1:6 (cement:lime:sand). Vertical pre-compression is applied to the columns 4 walls [5,16], with intensities between 4.4 % and 5 % of the column capacities. Finally, a vertical load equal to %1 of the compressive strength of masonry panels is placed on the top beam in 3 walls [5]. Due to the large scatter in the characteristics of the specimen studied, a cross-comparison between the findings of different studies is not possible. Therefore, only the individual findings of sensitivity analyses in each study regarding the changes in interaction effects due to variations in different parameters are explained in the following.

The numerical study in [38] inspect the influence of material properties and slenderness ratio. Compared to a benchmark squat wall (l/h=0.7, h/t = 25.4, and f'_m=2 MPa), the considered weaker- (f'_m= 1 MPa) and stronger-material (f'_m= 3.2 MPa) variants exhibit no different behavior under OOP/IP interaction. It is postulated that the adopted variation range is not wide enough to influence the interaction effects. On the other hand, the thicker (h/t = 20.6) and thinner (h/t = 46.3) specimens exhibit higher and lower OOP/IP interaction effects, respectively, compared to the original wall. All three walls exhibit similar IP strength drops until OOP pre-load up to 22 % of their strength, yet the thicker wall shows a more drastic performance degradation at higher pre-load. It loses half of its IP strength at an OOP pre-load level of 26 % of its original strength, while the original and the thinner wall exhibit such decrements at OOP pre-load levels of 65 % and 90 % of their strengths, respectively. The study employs a macro-element modeling approach and, therefore, does not provide auxiliary information regarding the damage patterns and the cause of the different behaviors. Nevertheless, it is assumed that the thicker walls experience more cracks during the OOP loading, which results in a higher IP strength drop compared to the thinner walls [38].

Another numerical study [5] investigates the influence of opening on the OOP/IP interaction in tall thin walls (l/h=2.2 and h/t = 24.1). They analyze the IP performance of 1 wall without opening, 1 wall with a door opening, and 1 partially filled frame (up to half of its height) under similar pre-applied OOP pressures. The wall with a door exhibits identical behavior to the full walls in terms of the amount and rate of IP strength drop with the increase of pre-load. The partial infill exhibits a lower sensitivity to pre-load, with a 20 % lower IP strength drop at the final pre-load level. This is because, according to [5], the contribution of the half-panel to the IP performance of the frame is already lower than that of the other walls, and the half-panel specimen exhibits a short-column effect that affects the IP behavior more than the OOP pre-load. Finally, the numerical study in [49] stipulates that anchoring the panels to the surrounding frame via steel bars running through horizontal mortar joints at different elevations can significantly reduce the OOP/IP interaction effects.

4.2.3. *Simultaneous OOP and IP loading*

The SM numerical simulation of [40] on 1 single-story single-bay wall (l/h=1.5 and h/t = 28) made with reinforced concrete frame and single-wythe hollow clay blocks laid with holes in horizontal direction (f'_m=2.4 MPa) and 1:1:6 (cement:lime:sand) mortar, shows even more severe interaction effects. The wall is subjected to 22 sets of bi-directional ground motions in double-clamped IP and two-way-bending OOP conditions under no vertical pre-compression.

The accelerograms of each ground motion set are scaled up to different intensities to perform an incremental dynamic analysis. The analyses are conducted with and without considering OOP/IP interaction effects. The curve presented in the corresponding publication draws the averaged backbone curve showing the maximum recorded IP drift (IDR) at different loading intestines (peak ground accelerations, or PGAs), with and without considering the influence of OOP behavior. The backbone curve without OOP/IP interaction effects exhibits linearly increasing IP drifts with the increase of loading intensity, reaching a maximum PGA of 3g at a 4.5 % IP drift level. Whereas, while the backbone curve of the case with interaction OOP/IP interaction effects starts the same linear proportionally between the IP drifts and loading intensities, it diverges from the linear curve at a PGA of 1.4g and reaches 4.5 % IP drift at a 37 % lower PGA (1.88g). The one with interaction effects also shows a 110 % larger IP drift at 2.1g compared to the case without interaction effects.

The other 3 SM numerical studies on the OOP/IP interaction effects [5,28,32] are conducted on 22 multi-story multi-bay frames rather than single walls. Nevertheless, they also show higher sensitivity of IP response to concurrent OOP load compared to pre-damage and pre-load.

The numerical investigation in [5] simulate 2 two-by-two (story--by-bay) reinforced concrete frames under four different real earthquakes (dynamic loading) with and without applying the OOP component of the load. The frames have similar geometries (average l/h=2.7 and 2.9 and h/t = 8.5 and 9.25 in the first- and second-story bays, respectively), and their panels are assembled via 300-mm-thick hollow clay blocks with vertical holes. One frame is fully infilled, while the bays of the other frame are partially filled up to 2/3 of their height. The fully infilled frame shows no sensitivity to interaction effects at low-intensity bi-directional loads (up to IP intensity of 0.45g). However, the behaviors diverge after this point, and the specimen shows as much as 55 % lower IP base shear and 55 % higher top IP drift under the highest intensity (0.81g in IP) bi-directional excitation compared to the unidirectional case. The partially-infilled panel shows a lower degradation of IP behavior, since, as explained before, its behavior is more governed by soft-story effects.

The numerical study in [28] considers 6 thick (h/t = 9.5) and 6 thin (h/t = 25.6) reinforced concrete frames with different number of stories and bays, under bi-directional QSM load (frame drift in IP and WFMiPL loading in OOP) with different proportionalities (OOP:IP load intensity ratios of 0.27, 0.58, 1.00, and 1.73). It is observed that thick specimens show only a slight 6 % IP performance degradation under the highest OOP:IP load proportion because they undergo minor OOP damage. At the same time, thin specimens show as much as 32 % IP strength drop and 47 % lower ultimate top IP drift capacity (corresponding to 20 % strength drop point) under the same loading conditions. The influence of OOP damage also diminishes with the decrease in aspect ratio. Meaning that, in the frames with thin walls, the tall specimen (five stories and two bays) shows 24 % and 15 % lower decrease in IP strength and drift capacity compared to the squat frame (two stories and five bays).

However, the 8 simulations of [32] on similarly thin (h/t = 26.1) frames with different aspect ratios (squat two-by-four to tall six-by-two story-by-bay configurations) under simultaneous QSM IP (frame drift) and OOP WFMiPL loading shows almost no interaction OOP/IP effects in the squat frame (two-by-four). Whereas the tallest specimen (six--by-two) exhibits as much as 50 % IP strength drop and 80 % lower ultimate IP drift capacity reduction under medium OOP load intensity (corresponding to an earthquake with intensity 0.3g). This contradictory observation may have arisen from the different OOP loading patterns adopted in the two studies, as the proportion between OOP and IP components of the lateral load are unclear in [32]. It is also shown in [32] that strengthening the infills with fiber- or steel-reinforced plasters can entirely neutralize the effects of OOP/IP interaction.

5. Available extrapolations of wall-level findings to the building-level response

The performance of masonry buildings under seismic load cannot be fully understood or improved without considering the interaction between OOP and IP behaviors [3,13–15]. This necessity has led to the development of analytical approaches to simulate masonry structures under these interaction effects, drawing from insights gained through wall-level studies. Unlike numerical and experimental methods, analytical models allow for the derivation of general principles applicable across various conditions [18]. By identifying key parameters influencing URM wall performance, they facilitate targeted interventions to enhance resilience. This section reviews the analytical approaches currently available in the literature that address IP-OOP interaction effects in framed unreinforced masonry constructions, detailing their methodologies.

5.1. Classification of currently available approaches

As the number of publications shown in Fig. 15 indicates, the analytical characterization of IP-OOP interaction effects has been pursued concurrently with the very first experimental and numerical studies. This is because analytical methods are particularly valuable in early-stage structural assessments, offering a cost-effective means to evaluate seismic vulnerability and retrofitting strategies. Hence, they are widely applied to the investigation of wall- or structural-level responses under IP-OOP interaction, as evidenced by at least 27 publications counted by this study [3,9,13–15,20,28–31,33–38,41,73,77,88,89,95,126–129]. Analytical approaches to IP-OOP interaction effects in URM walls can be broadly categorized into three types: regression-based formulations, mechanics-based models, and hybrid or semi-empirical models [89]. Specifically, 16 different regression-based formulas are presented in 17 publications [2,8,16,43,45,71,72,81,89,91,92,98,101,108,130–132], 1 of which [71] has already been adopted in the design and assessment guidelines since the year 1997. Moreover, 5 mechanics-based [32,38,117,133,134] and 7 hybrid [8,15,28,40,42,129,135] macro-element models are developed for framed structures. Regression-based developments are typically presented as predictive equations that estimate wall behavior under various loading scenarios without requiring full time-history simulations. Meanwhile, mechanics-based and hybrid models are primarily used to develop numerical methodologies

Regression-based formulations rely on statistical analyses of experimental or numerical data to establish relationships between interaction effects and key wall characteristics, such as material properties, geometry, and boundary conditions [18]. These models provide empirical equations or curves that directly correlate with observed behaviors, making them valuable for practical seismic assessments. Mechanics-based models, on the other hand, derive theoretical equations from fundamental physical principles to describe the responses of masonry walls under IP-OOP interaction. These models often involve simplifications, such as idealized failure mechanisms or localized failure zones, to make complex behaviors more tractable. While regression-based models offer practical design tools by leveraging large datasets, mechanics-based approaches provide deeper theoretical insights, enabling the development and refinement of assessment and design methodologies. Together, both approaches play crucial roles in seismic engineering, complementing each other in improving the understanding and prediction of URM wall performance.

However, developing robust regression-based equations or mechanics-based models presents significant challenges. A comprehensive dataset encompassing all parameters affecting interaction behaviors is currently lacking (See 3), making it difficult to achieve a statistically accurate representation of all possible failure modes. Additionally, the inherent heterogeneity of masonry materials and the anisotropic nature of their mechanical properties further complicate the formulation of

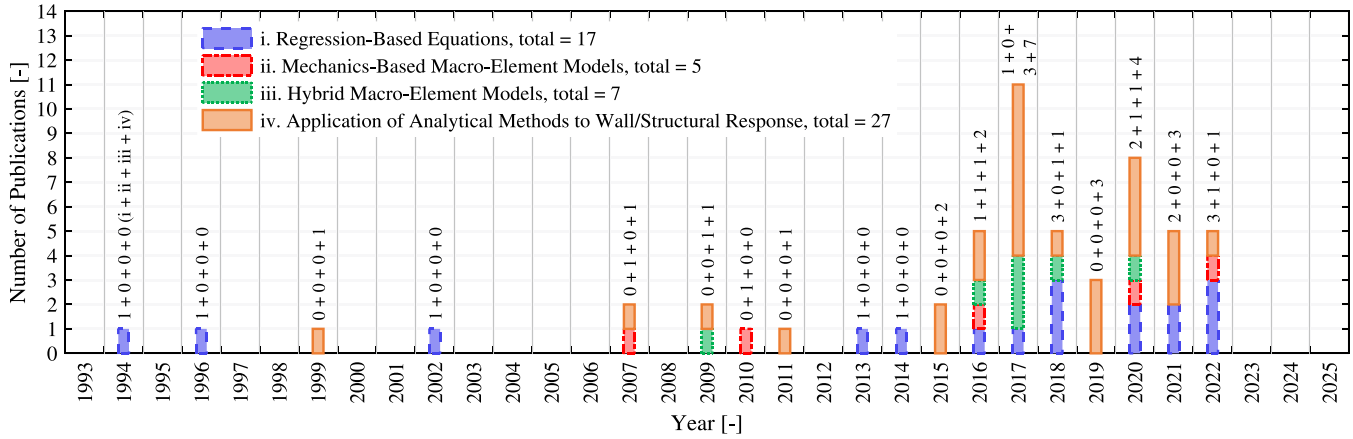

Fig. 15. Number of publications per year focusing on the analytical study of framed unreinforced masonry walls and structures under IP-OOP interaction effects. The papers are categorized based on the type of contribution, i.e. the development of an approach or the application of an already-developed approach.

reliable mechanics-based models. To address these limitations, hybrid or semi-empirical models integrate mechanics-based principles with empirical regression formulations, combining the strengths of both approaches. By calibrating theoretical predictions against observed data, these models refine and validate mechanics-based assumptions while maintaining the empirical accuracy of regression-based methods. This fusion enhances their ability to capture the complex reality of seismic behavior in URM walls.

5.2. Regression-based design and assessment formulas

The regression-based approaches developed for predicting IP–OOP interaction effects are summarized in Table 3. These are categorized based on the interaction scenario they address, the behavioral parameter

Table 3
Regression based analytical approaches for the prediction of IP-OOP interaction effects.

Interaction Scenario	Year	Publication(s)	Type	Changes in	Due to	Considering Sensitivities to	Used in Standards
IP/OOP	1994	Angel et al. [71,72]	Equation	OOP Strength	IP Pre-Damage	Critical IP Drift (Explicitly) Slenderness Ratio (Explicitly) Frame Stiffness (Explicitly)	FEMA 273 [137] (Constant) FEMA 356 [138] (Constant) ASCE 41 [140] (Constant) NZSEE [141] (Linearized) FEMA 306 [142] (Tabulated)
	2013	Morandi et al. [130]	Equation	OOP Strength OOP Stiffness	IP Pre-Damage	Critical IP Drift (Explicitly) Ultimate IP Drift (Explicitly)	–
	2014	Verlato et al. [131]	Equation	OOP Strength	IP Pre-Damage	Critical IP Drift (Explicitly) Ultimate IP Drift (Explicitly)	–
	2014	Cavaleri et al. [136]	Equation	OOP Strength OOP Stiffness	IP Pre-Damage	Critical IP Drift (Implicitly) Aspect Ratio (Implicitly) Slenderness Ratio (Implicitly) Masonry Material (Implicitly)	–
	2017	Wang [89]	Equation	OOP Strength	IP Pre-Damage	Ultimate IP Drift	–
	2018	Furtado et al. [2]	Equation	OOP Strength OOP Stiffness	IP Pre-Damage	Aspect Ratio (Implicitly) h/t (Implicitly)	–
	2018	Ricci et al. [91]	Equation	OOP Strength OOP Stiffness	IP Pre-Damage	Aspect Ratio (Implicitly)	–
	2018	Ricci et al. [92]	Equation	OOP Strength OOP Stiffness	IP Pre-Damage	Aspect (Implicitly) Slenderness Ratio (Implicitly)	
	2020	Nasiri & Liu [43]	Equation	OOP Strength	IP Pre-Damage	Aspect Ratio (Implicitly) Masonry Material (Implicitly)	–
	2020	Akhoundi et al. [98]	Equation	OOP Strength OOP Stiffness	IP Pre-Damage	–	–
	2021	Di Domenico et al. [101]	Equation	OOP Strength	IP Pre-Damage	Critical IP Drift (Explicitly) Aspect Ratio (Explicitly) Slenderness Ratio (Explicitly)	–
	2021	Xie et al. [108]	Equation	OOP Strength	IP Pre-Damage	Critical IP Drift (Explicitly) Aspect Ratio (Explicitly) Slenderness Ratio (Explicitly)	–
	2022	Morandi et al. [81]	Equation	OOP Strength OOP Stiffness	IP Pre-Damage	Critical IP Drift (Explicitly) Ultimate IP Drift (Explicitly) Slenderness Ratio (Implicitly)	–
OOP/IP	2002	Al Chaar et al. [132]	Interaction Curve	IP Strength	OOP Pre-Load	–	–
	2009	Kadysiewski and Mosalam [8]	Interaction Curve	IP Strength	OOP Pre-Load	–	ASCE 41 [140] (for SM loading)
	2016	Kong et al. [16]	Interaction Curve	IP Strength	OOP Pre-Load	–	–

modified due to interaction, the primary parameter used to quantify the modification, the additional parameters considered (either "explicitly" or "implicitly"), and their implementation in design and assessment standards. The "explicitly" term refers to cases where the parameter is directly included in the predictive equation, while the "implicitly" term indicates that, although the parameter is not explicitly represented, the equation is derived from datasets that include specimens exhibiting variations in that parameter.

Regarding IP/OOP interaction effects, several formulas have been proposed to calculate the reduction in OOP behavioral parameters as functions of changes in the IP response. Specifically, 14 studies [2,43,45,71,72,81,89,91,92,98,101,108,130,131] utilize outcomes from previous SQ studies to generate equations for the drop in OOP cracking and peak strength, as well as initial and secant stiffness (corresponding to the peak force) at different IP pre-damage levels. Other IP/OOP interaction scenarios (such as under SC, CB, or SM loading) are largely absent from the guidelines because they have not been sufficiently studied for the development of analytical formulations.

For the changes in OOP strength, the earliest development was proposed by Angel et al. [71,72], who suggested that IP/OOP interaction effects remain negligible as long as the panel does not crack under IP loading. Accordingly, they defined the OOP strength reduction factor as a function of the maximum IP drift normalized by the IP drift at which IP cracking initiates. A key ambiguity in this approach lies in the definition of cracking drift, as it is unclear whether it corresponds to the first visible cracks or major cracks. Since this parameter exhibits significant variability (ranging from 0.2 % to 0.65 % across different walls), it has been shown to substantially influence the predicted strength reduction rate [101]. More recent formulations refine this approach, allowing IP/OOP interaction to take effect at IP drifts as low as 0.14 %–0.2 % [2,91]. Di Domenico et al. [101] furthered previous developments by proposing a formula that calculates the critical IP drift based on the slenderness and aspect ratios of the walls, extending previous assumptions to accommodate both thick ($h/t < 10.0$) and thin ($h/t > 20.4$) walls, where critical IP drifts as high as 0.5 % have also been observed. Some other studies [43,81,89,98,131], however, take a more conservative stance and allow for OOP response degradation even with the slightest IP drift, disregarding the presence of a critical drift threshold.

Various mathematical functions have been employed to capture the progression of OOP strength degradation under IP/OOP interaction. Studies such as [89,98] propose a linearly increasing reduction factor calibrated from limited experimental data but lack validation against larger datasets. A piecewise step function is adopted in [130], where the OOP strength drops to 20 % of its initial value at 0.3 % IP drift, and remains constant until an ultimate 1.0 % IP drift, at which it drops to zero. This equation is based on tests on thin specimens ($h/t = 20.4$) and is overly conservative for thicker walls [92]. In the piecewise linear functions used in [43,81,131] the reduction factor linearly changes between specific values at pre-specified IP drifts. The parameters defining the functions of [81,131] are trained based on very specific experimental data points and fail to generalize across different wall types. For example, the curve in [131] is developed based on thick-wall data ($h/t = 8.8$) and underestimates the strength drop in thinner walls. The function in [43] incorporates a broader range of numerical data but is based on average behaviors across specimens with different geometrical and mechanical properties, limiting its ability to capture the influence of individual properties. Angel et al. [71,72] propose an exponential function that accounts for slenderness but suffers from poor calibration, leading to excessive strength reduction, particularly for more slender walls [41]. Ricci et al. [92] introduce a power function incorporating aspect ratio, which aligns well with squat walls ($1.3 < l/h < 1.5$) and slenderness ratios above 15. Di Domenico et al. [101] refine this approach using an extended dataset that includes square and thicker walls ($1.0 < l/h < 1.6$ and $h/t = 8.8$). Xie et al. [108] propose a simpler and more accurate equation that replaces height with diagonal span length in slenderness calculations, integrating aspect ratio implicitly rather than as an independent parameter.

While the abovementioned equations are not explicitly limited to an upper IP drift, they remain valid only up to a certain level of IP pre-damage level due to the absence of experimental or numerical data beyond this threshold. Consequently, studies typically restrict their methodologies to predefined ultimate IP pre-damage drift levels, typically ranging between 1 % and 1.5 %. Beyond this limit, different assumptions are made: some models set the OOP strength to zero [98,130,131], others maintain it at 40 % of the initial value [81], while certain formulations simply become undefined [101]. It should be noted that the influence of opening, frame material, and type of framed specimen (IM vs. CM) are not represented in these equations. Moreover, only [136] and [43] implicitly include the effect of masonry material properties.

In addition to OOP strength degradation under IP/OOP interaction, some studies propose models for estimating reductions in initial OOP stiffness and the stiffness at peak strength [2,81,91,92,98,136], following similar principles to those used for determining strength reduction. However, these formulations do not account for material variability, which could significantly affect the reduction in OOP behavioral parameters. Furthermore, no predictive models currently exist for estimating changes in ductility in pre-damaged walls. The absence of clear trends in ultimate OOP deformation, coupled with the force-controlled nature of the OOP loading phase in the tests, prevents the derivation of reliable equations for post-damage ductility.

Building codes and guidelines increasingly acknowledge the importance of IP/OOP interaction effects in design and safety assessments, yet they rarely provide explicit prescriptions. The only widely adopted formulation is the OOP strength reduction equation by Angel et al. [71], which has been incorporated into several seismic assessment standards. Due to the complexity of the original equation, a simplified version with a uniform 24 % reduction coefficient at all pre-damage levels was introduced in FEMA 273 [137] in 1997, and later retained in FEMA 356 [138] in 2000 and ASCE 41 [139] in 2006. A lower-bound alternative with a constant 40 % reduction factor was adopted in the 2017 revision of ASCE 41 [140]. The New Zealand NZSEE guideline [141] implements a linearized version that assigns a constant reduction factor based on the slenderness ratio. FEMA 306 [142] is the only standard that retains the original formulation, presenting the reduction factor in tabulated form based on the slenderness ratio and two levels of IP pre-damage: one moderate (corresponding to cracking) and the other severe (twice the cracking drift). However, regardless of its implementation, the equation of Angel et al. [71] significantly overestimates strength reduction due to its derivation for a representative slender strip under one-way bending, which neglects horizontal arching effects in two-way bending [101]. Moreover, it exhibits high variability and inconsistent predictions [88].

Regarding the OOP/IP interaction effects, 3 studies [16,132] propose regression-based equations for calculating the IP strength reduction due to OOP pre-load under CB loading scenario, although with very limited data to support their propositions. Kong et al. [16] derive interaction curves for IP strength reduction, based on numerical simulations of a single wall. Similarly, [132] presents a polynomial curve fitted to only two data points from numerical simulations. Finally, the ASCE 41 standard [140] adopts a 3/2-power interaction curve for specimens subjected to simultaneous IP and OOP load. However, this formulation, originally proposed by Kadysiewski and Mosalam [8], is based on numerical simulations of walls under OOP pre-load in the CB loading scenario, rather than the SM loading scenario. Moreover, the effect of no additional parameters is included in the development of these interaction curves.

5.3. *Macro-element numerical models capable of simulating IP-OOP interaction effects in buildings*

Although more detailed modeling strategies, such as those in [38,43,47,49–52,143], can effectively capture IP-OOP interaction effects and

are widely employed in wall-level investigations, their computational cost makes them impractical for large-scale structural analyses. Consequently, macro-element modeling has gained traction in recent years as an efficient alternative. Among the numerous macro-element models proposed in the literature, 11 instances [15,28,29,32,38,40,42,117,133,134,144] have been utilized in various studies [3,9,13,15,20,28–31,33–38,41,95,101,127,129,135] to capture IP-OOP interaction effects. These models employ different geometrical configurations and mechanical behaviors for the strut-and-tie systems that replace each masonry wall in the simulated building or frame. Due to space limitations, the presentation of such details is avoided, and only the classification of these models into three tiers based on their treatment of interaction effects is presented.

The first tier consists of the 5 mechanics-based models [32,38,117,133,134] that, while not explicitly designed for IP-OOP interaction, capture it as a byproduct of their mechanics-based approach. Three of these [32,117,134] replace masonry panels with planar braces, discretizing each strut into multiple fibers stacked along height and thickness. The fiber-level mechanical properties are calibrated so that the entire brace replicates both IP and OOP behaviors of the original wall. This enables localized damage in individual fibers, leading to realistic strength degradation under combined loading conditions. In the fourth model [133], the panel is discretized into several rigid trusses connected to a central single-fiber truss element. The central element is assigned different nonlinear behaviors in IP and OOP directions, which are linked via a mutual damage parameter. The fifth model [38] employs a 3D brace configuration instead of a planar one, using single-fiber truss elements arranged in a non-planar layout. This configuration naturally develops resistance to both IP and OOP load, allowing the model to capture interaction effects under different loading scenarios.

The second tier includes 3 models [28,29,135] that extend the models of the previous tier by incorporating interaction effects through element removal techniques. In these models, the struts and ties of each masonry panel are removed once failure of the corresponding panel occurs in either the IP or OOP direction. IP and OOP yield and failure thresholds are determined using empirically based interaction laws, such as the 3/2-power formulation proposed in [8] or similar linearized criteria [135]. Hence, this tier belongs to the category of hybrid analytical approaches. It should be noted that the model developed in [28] only applies element removal when the OOP displacement threshold is reached, considering only the OOP/IP interaction effects. The remaining models consider thresholds for both IP and OOP deformation.

The third tier comprises 4 additional hybrid models [15,40,42,144] that further integrate IP and OOP behaviors by dynamically modifying the parameters defining the constitutive IP behaviors during the simulation based on the extent of OOP damage and vice versa. Reduction factors for the IP and OOP constitutive behavioral parameters are derived from empirical equations based on single-wall experiments or numerical simulations conducted under IP pre-damage and sequential loading. However, since these models are applied to structures subjected to bidirectional seismic loading, their empirical reduction laws may not fully capture the complexities of simultaneous loading effects. Notably, one of these models [42] accounts only for IP/OOP interactions, disregarding OOP/IP interaction effects, limiting its applicability in certain scenarios.

6. Current knowledge gaps in the study of interaction effects in framed URM walls

The literature on framed URM walls subjected to IP-OOP interaction has grown in recent years; however, several critical gaps continue to hinder confident prediction and design. The available experimental and numerical data remain scattered across loading scenarios and specimen configurations, while many analytical developments are based on limited datasets. Consequently, the extrapolation of wall-level findings to frame- or building-scale applications remains only partially validated. Additionally, the lack of consistent terminology for interaction types and loading scenarios has impeded coherent comparison across studies and modeling approaches. Addressing these limitations requires targeted experimental efforts, clearly documented loading protocols, and analytical or numerical tools calibrated against broader datasets that reflect realistic boundary conditions and geometrical configurations. The following sections outline the key knowledge gaps identified in this review.

6.1. Scientific gaps in understanding the interaction effects

Research attention remains uneven across interaction types and governing parameters. The emphasis is predominantly on IP/OOP interaction effects, whereas OOP/IP interaction is supported by comparatively few studies. Most experimental data are gathered from the SQ loading scenario, while data regarding the other scenarios, especially SM which is most representative of realistic seismic loading conditions is sparse. Slenderness ratio (h/t) is consistently identified as the dominant driver of OOP degradation after IP damage, but reported trends include contradictions. Aspect ratio (l/h) influences failure mode and arching activation, yet cross-study consistency is limited. The influence of openings and multi-bay behaviors are also underrepresented. Scale effects on IP-OOP interaction remain unexplored. A significant lack of data is also highlighted for CM walls despite their different response to IP-OOP interactions compared to IM walls. The role of frame material on the interaction effects is also not investigated.

6.2. Limitations in experimental, numerical, and analytical methodologies

The available dataset is skewed. Over 90 % of tested framed specimens are IM walls, while CM walls are rarely considered. Multi-bay frames are scarcely represented, and openings appear in only six tested panels across all experimental campaigns. Most tests are carried out considering IP/OOP interaction and employ the SQ loading scenario, with limited representation of full SM loading. Moreover, loading histories are often restricted to simple QSM loading. Many specimens are single-wythe, and the role of cavities or multiple wythes is inconsistently addressed, leading to inconclusive findings. Experimental campaigns involving scaled specimens do not include full-scale counterparts, preventing any meaningful investigation of scale effects. Numerical models are typically calibrated against a small set of benchmark experiments, and their findings cannot be reliably generalized to a broader range of structural configurations. On the analytical and numerical side, commonly used IP/OOP reduction equations are validated only up to 1–1.5 % IP drift. Beyond this range, studies often adopt incompatible assumptions, such as zero residual capacity or fixed residual fractions, and no predictive models currently exist for post-damage ductility. Furthermore, the IP drift threshold at which IP/OOP interaction effects initiate varies widely (0.2–0.65 %) and lacks a uniform definition, resulting in significant discrepancies in strength-loss predictions. At the building scale, detailed continuum or fine-resolution models are capable of capturing interaction effects but are computationally intensive. Macro-element approaches offer reduced computational cost, yet many rely on empirical reductions derived from limited SQ testing and often fail to capture SM loading effects. In some cases, OOP/IP interaction is entirely omitted, further limiting the applicability of such models under true bidirectional loading conditions.

6.3. Practical gaps in design and assessment guidelines

Design and assessment provisions acknowledge the influence of IP-OOP interaction. However, the analytical equations they implement remain calibrated on narrow datasets and omit several key governing variables identified at the wall level. A primary limitation concerns the dependence on loading scenario. Most regression-based formulations

are calibrated using SQ loading data, and even where SM curves are cited in practice (e.g., a 3/2-power relationship), they are effectively derived from CB loading datasets. A second limitation lies in the treatment of interaction types within modeling frameworks. While several building-scale macro-element implementations account for IP/OOP effects, they often exclude OOP/IP interactions and therefore cannot capture the reduction in IP strength or stiffness caused by prior or concurrent OOP actions. A third constraint relates to boundary conditions embedded within the reduction equations. The most widely adopted formulation [71,72] is calibrated for one-way bending, thereby neglecting horizontal arching effects under two-way bending conditions. When these equations are further simplified in code applications to depend primarily on slenderness, the exclusion of two-way effects is effectively preserved, introducing bias in cases where arching significantly contributes to the OOP response. A fourth and equally significant limitation pertains to the representation of material properties. Commonly used interaction reductions emphasize geometric parameters, particularly slenderness ratio, and occasionally aspect ratio and IP pre-damage drift, but omit unit and mortar strength, bond quality, and masonry typology as explicit variables. These material characteristics have been shown to substantially influence masonry bond and, in turn, seismic response [145,146]. Other key factors, such as the presence and configuration of openings, the number of wythes, and the distinctions between CM and IM behavior, are also entirely absent from current formulations.

7. Conclusions

This paper presents a comprehensive dataset of the studies available in the literature on the influence of interaction between in-plane (IP) and out-of-plane (OOP) behaviors on the response of framed unreinforced (URM) masonry. The findings of currently published experimental and numerical investigations on IP-OOP interaction effects in infill and confined masonry walls are reviewed, and key factors influencing IP-OOP interaction, including geometric configurations, material properties, boundary conditions, and loading scenarios, as well as areas requiring further investigation are identified. The state-of-the-art analytical equations and macro-element models developed based on wall-level studies for the purpose of estimating the behavior of larger structures, such as multi-bay multi-story frames and complete buildings, are reviewed, and knowledge gaps are highlighted. The main findings of the paper are summarized as follows:

- The studies on IP-OOP interaction in framed URM walls do not follow a consistent terminology, which has led to inconsistent use of terms for fundamentally different interaction scenarios. To address this, the present study introduces a unified classification system with consistent terminology to clearly define and distinguish various types of IP-OOP interactions.
- The review highlights the scarcity of experimental and numerical investigations on IP-OOP interaction effects. Existing studies often focus on isolated conditions, limiting their applicability to broader structural assessments.
- While both IP/OOP and OOP/IP interactions influence the seismic performance of framed masonry structures, the majority of existing studies focus on IP/OOP effects, where prior in-plane damage weakens the out-of-plane capacity. The influence of wall geometry, boundary conditions, and loading conditions, as well as material properties, requires further experimental and numerical validation.
- Regarding IP/OOP interaction effects, the slenderness ratio is the most critical factor. Slender walls ($h/t > 20$) suffer pronounced strength degradation under IP pre-damage, due to increased instability and lower arching effects, while squat walls ($h/t < 10$) show more stable OOP behavior. Aspect ratio follows, affecting failure modes and load distribution, particularly in tall walls ($l/h<1.0$) where horizontal arching action plays a significant role in the OOP behavior. However, studies on aspect ratio effects remain inconsistent, highlighting the need for further targeted investigations.
- Other parameters less investigated experimentally yet significantly influencing IP/OOP interaction effects include the material properties of masonry panels and the flexibility of the surrounding frame. Masonry material properties, including the compressive strength, unit type, and bond quality, govern crack initiation and propagation under interaction effects. Panels with either very strong or very weak materials show higher sensitivity to IP pre-damage compared to intermediate-strength panels, due to crack localization in areas that coincide with OOP damage paths. Frame type also affects the composite action of the wall, with steel frames showing greater susceptibility to interaction effects due to cracking at the frame-panel interface when pre-damaged in IP.
- Even less studied, yet potentially impactful, parameters influencing IP/OOP interaction include the presence and arrangement of openings, which disrupt load paths and introduce localized weaknesses, and the behavior of multi-bay and multi-story frames, where interaction effects accumulate across structural components, altering the global response mechanisms.
- Analytical equations developed for larger structures primarily focus on the sequential effects of IP pre-damage on OOP response. Although many of these models incorporate the effects of wall parameters, such as slenderness, aspect ratio, and boundary conditions, they rely on limited datasets, which hinders their predictive capability for broader applications.
- Current seismic guidelines acknowledge IP-OOP interactions but provide minimal design prescriptions. The equation by Angel et al. [71], widely adopted in codes, tends to overestimate strength degradation due to its simplified assumptions.

Despite significant progress in understanding IP-OOP interaction effects, several critical research gaps remain. More systematic investigations are required to establish a comprehensive understanding of interaction mechanisms and to consistently evaluate the influence of key parameters, particularly slenderness ratio, aspect ratio, frame flexibility, and the presence of openings, on IP-OOP interaction effects. The masonry bond pattern is another parameter requiring more investigation. Although numerical models, especially macro-element ones, offer valuable insights, their reliability should be improved through calibration and validation against a broader range of experimental data. The development and incorporation of more robust design and assessment equations, grounded in the more realistic SM loading scenario and including more structural properties, into guidelines will be essential for advancing reliable assessment and retrofitting strategies for masonry buildings in seismic regions.

CRediT authorship contribution statement

Amirhossein Ghezelbash: Writing – review & editing, Writing – original draft, Visualization, Validation, Resources, Methodology, Investigation, Formal analysis, Data curation, Conceptualization. **Jan G. Rots:** Writing – review & editing, Validation, Supervision, Project administration, Funding acquisition, Conceptualization. **Francesco Messali:** Writing – review & editing, Validation, Supervision, Resources, Project administration, Methodology, Funding acquisition, Data curation, Conceptualization.

Funding

This research was conducted as part of the scientific consolidation of projects funded by Nederlandse Aardolie Maatschappij (NAM) BV under contract number UI46268 “Physical testing and modeling–Masonry structures Groningen”, which is gratefully acknowledged.

Declaration of Competing Interest

The authors declare that they have no known competing financial interests or personal relationships that could have appeared to influence the work reported in this paper.

Acknowledgements

The data used in this paper are gathered from the relevant studies published in literature. References to the studies corresponding to each portion of the text are made in the manuscript.

References

[1] Bojadjiev J, Apostolska R, Necevska Cvetanovska G, Varevac D, Bojadjieva J. Experimental verification of innovative, Low-Cost method for upgrading of seismic resistance of masonry infilled rc frames. Appl Sci 2025;15:8520. https://doi.org/10.3390/app15158520.
[2] Furtado A, Rodrigues H, Arêde A, Varum H. Out-of-plane behavior of masonry infilled RC frames based on the experimental tests available: a systematic review. Constr Build Mater 2018;168:831–48. https://doi.org/10.1016/j.conbuildmat.2018.02.129.
[3] Longo F, Wiebe L, da Porto F, Modena C. Application of an In-Plane/Out-Of-Plane interaction model for URM infill walls to dynamic seismic analysis of RC frame buildings. Bull Earthq Eng 2018;16:6163–90. https://doi.org/10.1007/s10518-018-0439-0.
[4] Sattar S, Liel AB. Seismic performance of nonductile reinforced concrete frames with masonry infill Walls—I: development of a strut model enhanced by finite element models. Earthq Spectra 2016;32:795–818. https://doi.org/10.1193/090914eqs139m.
[5] Yuen TYP, Kuang JS, Ali BSM. Assessing the effect of bi-directional loading on nonlinear static and dynamic behaviour of masonry-infilled frames with openings. Bull Earthq Eng 2016;14:1721–55. https://doi.org/10.1007/s10518-016-9899-2.
[6] Dias-Oliveira J, Rodrigues H, Asteris P, Varum H. On the seismic behavior of masonry infilled frame structures. Buildings 2022;12:1146. https://doi.org/10.3390/buildings12081146.
[7] Zhang M, Ding J, Jin W, Ding K, Ren M. Study on in-plane/out-of-plane seismic performance of masonry-infilled RC frame with openings and a new type of flexible connection. Bull Earthq Eng 2024;22:2201–33. https://doi.org/10.1007/s10518-024-01855-7.
[8] Kadysiewski S., Mosalam K.M. Modeling of unreinforced masonry infill walls considering in-plane and out-of-plane interaction. Berkeley, CA, USA: 2009.
[9] Mazza F, Donnici A. In-plane-out-of-plane single and mutual interaction of masonry infills in the nonlinear seismic analysis of RC framed structures. Eng Struct 2022;257:114076. https://doi.org/10.1016/j.engstruct.2022.114076.
[10] Dias-Oliveira J, Rodrigues H, Asteris P, Varum H. On the seismic behavior of masonry infilled frame structures. Buildings 2022;12:1146. https://doi.org/10.3390/buildings12081146.
[11] Baek ER, Pohoryles DA, Bournas D. Seismic assessment of the in-plane/out-of-plane interaction of masonry infills in a two-storey RC building subjected to bi-directional shaking table tests. Earthq Eng Struct Dyn 2024;53:2230–51. https://doi.org/10.1002/eqe.4109.
[12] Fardis MN, Bousias SN, Franchioni G, Panagiotakos TB. Seismic response and design of RC structures with plan-eccentric masonry infills. Earthq Eng Struct Dyn 1999;28:173–91. https://doi.org/10.1002/(SICI)1096-9845(199902)28:2<173::AID-EQE810>3.0.CO;2-1.
[13] Pradhan B, Sarhosis V, Ferrotto MF, Penava D, Cavaleri L. Prediction equations for Out-of-Plane capacity of unreinforced masonry infill walls based on a macroelement model parametric analysis. J Eng Mech 2021;147. https://doi.org/10.1061/(ASCE)EM.1943-7889.0001998.
[14] Ricci P, Di Domenico M, Verderame GM. Effects of the In-Plane/Out-of-Plane interaction in URM infills on the seismic performance of RC buildings designed to eurocodes. J Earthq Eng 2022;26:1595–629. https://doi.org/10.1080/13632469.2020.1733137.
[15] Gesualdi G, Viggiani LRS, Cardone D. Seismic performance of RC frame buildings accounting for the out-of-plane behavior of masonry infills. Bull Earthq Eng 2020;18:5343–81. https://doi.org/10.1007/s10518-020-00904-1.
[16] Kong J, Zhai C, Wang X. In-Plane behavior of masonry infill wall considering Out-of-Plane loading. Period Polytech Civ Eng 2016;60:217–21. https://doi.org/10.3311/PPci.7867.
[17] Pradhan B, Zizzo M, Sarhosis V, Cavaleri L. Out-of-plane behaviour of unreinforced masonry infill walls: review of the experimental studies and analysis of the influencing parameters. Structures 2021;33:4387–406. https://doi.org/10.1016/j.istruc.2021.07.038.
[18] Ghezelbash A, Rots JG, Messali F. Review of the influence of the interaction between In-Plane and Out-of-Plane behaviors on the seismic response of Non-Framed unreinforced masonry walls. Buildings 2025;15:2874. https://doi.org/10.3390/buildings15162874.
[19] Franza A, Miraei S, Boldini D, Losacco N. An equivalent beam approach for assessing tunnelling-induced distortions of frames with infills. Tunn Undergr Space Technol 2022;129:104686. https://doi.org/10.1016/j.tust.2022.104686.
[20] Mazza F, Donnici A. In-plane and out-of-plane seismic damage of masonry infills in existing r.c. Structures: the case study of de Gasperi-Battaglia school in norcia. Bull Earthq Eng 2021;19:345–76. https://doi.org/10.1007/s10518-020-00981-2.
[21] Thomoglou AK, Jagadesh P, Voutetaki ME. Review of Out-of-Plane strengthening techniques of unreinforced masonry walls. Fibers 2023;11:78. https://doi.org/10.3390/fib11090078.
[22] Dauda JA, Iuorio O, Muhit IB, da Silva LCM. Systematic review of experimental testing of masonry walls' failure: comparative analysis and future directions. Eng Fail Anal 2024;163:108571. https://doi.org/10.1016/j.engfailanal.2024.108571.
[23] Chewe Ngapeya GG, Waldmann D, Scholzen F. Impact of the height imperfections of masonry blocks on the load bearing capacity of dry-stack masonry walls. Constr Build Mater 2018;165:898–913. https://doi.org/10.1016/j.conbuildmat.2017.12.183.
[24] Rai DC, Singhal V, Raj SB, Sagar SL. Reconnaissance of the effects of the M7.8 gorkha (Nepal) earthquake of April 25, 2015. Geomat Nat Hazards Risk 2016;7:1–17. https://doi.org/10.1080/19475705.2015.1084955.
[25] Ghezelbash A, D'Altri AM, Sharma S, Lourenço PB, Rots JG, Messali F. A block-based numerical strategy for modeling the dynamic out-of-plane behavior of unreinforced brick masonry walls. Meccanica 2024. https://doi.org/10.1007/s11012-024-01899-8.
[26] Dhanasekar M, Page AW, Kleeman PW. The failure of brick masonry under biaxial stresses. Proc Inst Civ Eng 1985;79:295–313. https://doi.org/10.1680/iicep.1985.992.
[27] Singhal V, Rai DC. Role of toothing on In-Plane and Out-of-Plane behavior of confined masonry walls. J Struct Eng 2014;140. https://doi.org/10.1061/(ASCE)ST.1943-541X.0000947.
[28] Donà M, Tecchio G, Domenicale L, Saler E, Minotto M, da Porto F. Directional effects on combined In-Plane and out of plane seismic behavior of masonry infills. 6th ECCOMAS Thematic Conference on Computational Methods in Structural Dynamics and Earthquake Engineering (COMPDYN). Athens: Institute of Structural Analysis and Antiseismic Research School of Civil Engineering National Technical University of Athens (NTUA) Greece; 2017. p. 3332–51. https://doi.org/10.7712/120117.5649.18570.
[29] Mosalam KM, Günay S. Progressive collapse analysis of reinforced concrete frames with unreinforced masonry infill walls considering In-Plane/Out-of-Plane interaction. Earthq Spectra 2015;31:921–43. https://doi.org/10.1193/062113EQS165M.
[30] Han J, Zhang Z, Huang L, Sun X. Influence of In-Plane and Out-of-Plane interaction of infill walls on global collapse resistance capacity of infilled RC frame. 6th International Conference on Computational Methods in Structural Dynamics and Earthquake Engineering (COMPDYN). Athens, Greece: Institute of Structural Analysis and Antiseismic Research School of Civil Engineering National Technical University of Athens (NTUA) Greece; 2017. p. 3398–405. https://doi.org/10.7712/120117.5653.18616.
[31] Longo F. Numerical modelling of unreinforced masonry infill walls under seismic load considering in-plane/out-of-plane interaction. Italy: University of Trento; 2016.
[32] Donà M, Minotto M, Verlato N, da Porto F. A new macro-model to analyse the combined in-plane/out-of-plane behaviour of unreinforced and strengthened infill walls. Eng Struct 2022;250:113487. https://doi.org/10.1016/j.engstruct.2021.113487.
[33] Albano M, Gesualdi G, Viggiani LRS, Cardone D. Seismic response of RC frame buildings considering In-Plane and Out-of-Plane behaviour of unreinforced masonry infills. In: Wang CM, Dao V, Kitipornchai S, editors. EASEC16, Lecture Notes in Civil Engineering 101, 101. Singapore: Springer Singapore; 2021. p. 1595–605. https://doi.org/10.1007/978-981-15-8079-6_147.
[34] Furtado A, Rodrigues H, Arêde A, Varum H. Influence of the In-Plane and Out-of-Plane masonry infill Walls' interaction in the structural response of RC buildings. 1st International Conference on Structural Integrity Influence, 114. Funchal, Madeira, Portugal: Elsevier Ltd; 2015. p. 722–9. https://doi.org/10.1016/j.proeng.2015.08.016.
[35] Mazza F, Donnici A. Effects of In- and Out-of-Plane nonlinear modelling of masonry infills on the seismic response of R.C. Framed buildings. 24th Conference of the Italian Association of Theoretical and Applied Mechanics. Rome, Italy: Springer Science and Business Media Deutschland GmbH; 2020. p. 1838–56. https://doi.org/10.1007/978-3-030-41057-5_148.
[36] Al Hanoun MH, Abrahamczyk L, Schwarz J. Macromodeling of in- and out-of-plane behavior of unreinforced masonry infill walls. Bull Earthq Eng 2019;17:519–35. https://doi.org/10.1007/s10518-018-0458-x.
[37] Kadysiewski S., Mosalam K.M. Modelling of Unreinforced Masonry Infill Walls Considering In-Plane and Out-of-Plane Interaction. 11th Canadian Masonry Symposium, Toronto, Ontario, Canada: 2009.
[38] Hashemi A, Mosalam KM. Seismic evaluation of reinforced concrete buildings including effects of masonry infill walls. Berkeley. Berkeley, CA, USA: PEER Report 2007/100 Pacific Earthquake Engineering Research Center College of Engineering, University of California; 2007.
[39] Bahreini V, Mahdi T, Najafizadeh MM. Evaluation of brick infill walls under in-plane and out-of-plane loading. J Vibroengineering 2017;19:394–408. https://doi.org/10.21595/jve.2016.17259.
[40] Di Domenico M, Ricci P, Verderame GM. Empirical unreinforced masonry infill Macro-Model accounting for In-Plane/Out-of-Plane interaction. 6th International Conference on Computational Methods in Structural Dynamics and Earthquake Engineering (COMPDYN. Athens: Institute of Structural Analysis and Antiseismic Research School of Civil Engineering National Technical University of Athens (NTUA) Greece; 2017. p. 1606–24. https://doi.org/10.7712/120117.5516.17533.

[41] Di Trapani F, Shing PB, Cavaleri L. Macroelement model for In-Plane and Out-of-Plane responses of masonry infills in frame structures. J Struct Eng 2018;144. https://doi.org/10.1061/(ASCE)ST.1943-541X.0001926.

[42] Mazza F. In-plane-out-of-plane non-linear model of masonry infills in the seismic analysis of r.c.-framed buildings. Earthq Eng Struct Dyn 2018;48:432–53. https://doi.org/10.1002/eqe.3143.

[43] Nasiri E, Liu Y. Effect of prior in-plane damage on the out-of-plane performance of concrete masonry infills. Eng Struct 2020;222:111149. https://doi.org/10.1016/j.engstruct.2020.111149.

[44] Wang X, Zhao W, Kong J, Zhao T. Numerical investigation on the influence of In-Plane damage on the Out-of-Plane behavior of masonry infill walls. Adv Civ Eng 2020;2020:1–16. https://doi.org/10.1155/2020/6276803.

[45] Cavaleri L, Zizzo M, Asteris PG. Residual out-of-plane capacity of infills damaged by in-plane cyclic loads. Eng Struct 2020;209:109957. https://doi.org/10.1016/j.engstruct.2019.109957.

[46] D'Altri AM, Sarhosis V, Milani G, Rots J, Cattari S, Lagomarsino S, et al. Modeling strategies for the computational analysis of unreinforced masonry structures: review and classification. Arch Comput Methods Eng 2020;27:1153–85.

[47] Mohyeddin A, Goldsworthy HM, Gad EF. FE modelling of RC frames with masonry infill panels under in-plane and out-of-plane loading. Eng Struct 2013;51:73–87. https://doi.org/10.1016/j.engstruct.2013.01.012.

[48] D'Altri AM, de Miranda S, Castellazzi G, Sarhosis V. A 3D detailed micro-model for the in-plane and out-of-plane numerical analysis of masonry panels. Comput Struct 2018;206:18–30. https://doi.org/10.1016/j.compstruc.2018.06.007.

[49] Yuen TYP, Kuang JS. Masonry-Infilled RC frames subjected to combined In-Plane and Out-of-Plane loading. Int J Struct Stab Dyn 2014;14:1350066. https://doi.org/10.1142/S0219455413500661.

[50] Zhai C, Kong JC, Wang XH. A finite element model for simulating Out-of-Plane behavior of masonry infilled RC frames. Appl Mech Mater 2012;166–169:849–52. https://doi.org/10.4028/www.scientific.net/AMM.166-169.849.

[51] Bahreini V, Mahdi T, Najafizadeh MM. Numerical study on the In-Plane and Out-of-Plane resistance of brick masonry infill panels in steel frames. Shock Vib 2017;2017:1–16. https://doi.org/10.1155/2017/8494657.

[52] Nasiri E, Liu Y. Development of a detailed 3D FE model for analysis of the in-plane behaviour of masonry infilled concrete frames. Eng Struct 2017;143:603–16. https://doi.org/10.1016/j.engstruct.2017.04.049.

[53] Nasiri E, Liu Y. The out-of-plane behaviour of concrete masonry infills bounded by reinforced concrete frames. Eng Struct 2019;184:406–20. https://doi.org/10.1016/j.engstruct.2019.01.098.

[54] van Zijl GPAG. Computational modelling of masonry creep and shrinkage. Delft University of Technology; 2000.

[55] Macorini L, Izzuddin BA. A non-linear interface element for 3D mesoscale analysis of brick-masonry structures. Int J Numer Methods Eng 2011;85:1584–608. https://doi.org/10.1002/nme.3046.

[56] Aref AJ, Dolatshahi KM. A three-dimensional cyclic meso-scale numerical procedure for simulation of unreinforced masonry structures. Comput Struct 2013;120:9–23. https://doi.org/10.1016/j.compstruc.2013.01.012.

[57] D'Altri AM, Messali F, Rots J, Castellazzi G, de Miranda S. A damaging block-based model for the analysis of the cyclic behaviour of full-scale masonry structures. Eng Fract Mech 2019;209:423–48. https://doi.org/10.1016/j.engfracmech.2018.11.046.

[58] Zeng B, Li Y, Noguez CC. Modeling and parameter importance investigation for simulating in-plane and out-of-plane behaviors of un-reinforced masonry walls. Eng Struct 2021;248:113233. https://doi.org/10.1016/j.engstruct.2021.113233.

[59] Nie Y, Sheikh A, Griffith M, Visintin P. A damage-plasticity based interface model for simulating in-plane/out-of-plane response of masonry structural panels. Comput Struct 2022;260:106721. https://doi.org/10.1016/j.compstruc.2021.106721.

[60] Oktiovan YP, Messali F, Pulatsu B, Lemos JV, Rots JG. A contact-based constitutive model for the numerical analysis of masonry structures using the distinct element method. Comput Struct 2024;303:107499. https://doi.org/10.1016/j.compstruc.2024.107499.

[61] Nie Y, Sheikh A, Visintin P, Griffith M. A robust computational strategy for failure prediction of masonry structures using an improved multi-surface damage-plastic based interface model. Int J Numer Methods Eng 2023;124:2498–528. https://doi.org/10.1002/nme.7218.

[62] Li Y, Zeng B. Modeling of masonry structures using a new 3D cohesive interface material model considering dilatancy softening. Eng Struct 2023;277:115466. https://doi.org/10.1016/j.engstruct.2022.115466.

[63] Baraldi D, Cecchi A. A full 3D rigid block model for the collapse behaviour of masonry walls. Eur J Mech A/Solids 2017;64:11–28. https://doi.org/10.1016/j.euromechsol.2017.01.012.

[64] Bui TT, Limam A, Sarhosis V, Hjiaj M. Discrete element modelling of the in-plane and out-of-plane behaviour of dry-joint masonry wall constructions. Eng Struct 2017;136:277–94. https://doi.org/10.1016/j.engstruct.2017.01.020.

[65] Smoljanović H, Živaljić N, Nikolić Ž, Munjiza A. Numerical analysis of 3D dry-stone masonry structures by combined finite-discrete element method. Int J Solids Struct 2018;136–137:150–67. https://doi.org/10.1016/j.ijsolstr.2017.12.012.

[66] Milani G. 3D upper bound limit analysis of multi-leaf masonry walls. Int J Mech Sci 2008;50:817–36. https://doi.org/10.1016/j.ijmecsci.2007.11.003.

[67] Tiberti S, Milani G. 3D homogenized limit analysis of non-periodic multi-leaf masonry walls. Comput Struct 2020;234:106253. https://doi.org/10.1016/j.compstruc.2020.106253.

[68] Khattak N, Derakhshan H, Thambiratnam DP, Malomo D, Perera NJ. Modelling the in-plane/out-of-plane interaction of brick and stone masonry structures using applied element method. J Build Eng 2023;76:107175. https://doi.org/10.1016/j.jobe.2023.107175.

[69] Lourenço PB, Rots JG, Blaauwendraad J. Continuum model for masonry: parameter estimation and validation. J Struct Eng 1998;124:642–52. https://doi.org/10.1061/(ASCE)0733-9445(1998)124:6(642).

[70] Vanin F, Penna A, Beyer K. A three-dimensional macroelement for modelling the in-plane and out-of-plane response of masonry walls. Earthq Eng Struct Dyn 2020;49:1365–87. https://doi.org/10.1002/eqe.3277.

[71] Angel R, Abrams D, Shapiro D, Uzarski J, Webster M. Behavior of reinforced concrete frames with masonry infills. Department of Civil Engineering, University of Illinios; 1994.

[72] Abrams DP, Angel R, Uzarski J. Out-of-Plane strength of unreinforced masonry infill panels. Earthq Spectra 1996;12:825–44. https://doi.org/10.1193/1.1585912.

[73] Flanagan RD, Bennett RM. Bidirectional behavior of structural clay tile infilled frames. J Struct Eng 1999;125:236–44. https://doi.org/10.1061/(ASCE)0733-9445(1999)125:3(236).

[74] Calvi GM, Bolognini D. Seismic response of reinforced concrete frames infilled with weakly reinforced masonry panels. J Earthq Eng 2001;5:153–85. https://doi.org/10.1080/13632460109350390.

[75] Rai DC, Komaraneni S, Singhal V. Out-of-plane seismic behaviour of brick masonry infilled panels with prior in-plane damage. 11th Canadian Masonry Symposium. Toronto, Ontario, Canada: Canadian Masonry Design Centre; 2009.

[76] Pereira MFP, Pereira MFN, Ferreira JED, Lourenço PB. Behavior of damaged masonry infill panels in RC frames subjected to out of plane loads. 7th International Conference Analytical Models and New Concepts in Concrete and Masonry Structures (AMCM2011, 5. Cracow, Poland: Faculty of Civil Engineering, Cracow University of Technology; 2011. p. 83–98.

[77] Komaraneni S, Rai DC, Singhal V. Seismic behavior of framed masonry panels with prior damage when subjected to Out-of-Plane loading. Earthq Spectra 2011;27:1077–103. https://doi.org/10.1193/1.3651624.

[78] da Porto F., Guidi G., Benetta M.D., Verlato N. Combined In-Plane/Out-of-Plane Experimental Behaviour of Reinforced and Strengthened Infill Masonry Walls. 12th Canadian Masonry Symposium, Vancouver, British Columbia, Canada: 2013, p. 1–11.

[79] Guidi G., da Porto F., Dalla Benetta M., Verlato N., Modena C. Comportamento Sperimentale nel Piano e Fuori Piano di Tamponamenti in Muratura Armata e Rinforzata. XV Convegno Nazionale ANIDIS - "L'Ingegneria Sismica in Italia," Padova, Italy: 2013, p. 9.

[80] Hak S, Morandi P, Magenes G. Out-of-Plane experimental response of strong masonry infills. 2nd European Conference on Earthquake Engineering and Seismology. Istanbul, Turkey: Kandilli Observatory And Earthquake Research Institute; 2014. p. 1–12.

[81] Morandi P, Hak S, Milanesi RR, Magenes G. In-plane/out-of-plane interaction of strong masonry infills: from cyclic tests to out-of-plane verifications. Earthq Eng Struct Dyn 2022;51:648–72. https://doi.org/10.1002/eqe.3584.

[82] Milanesi RR, Morandi P, Manzini CF, Albanesi L, Magenes G. Out-of-plane response of an innovative masonry infill with sliding joints from shaking table tests. J Earthq Eng 2022;26:1789–823. https://doi.org/10.1080/13632469.2020.1739173.

[83] da Porto F, Guidi G, Verlato N, Modena C. Effectiveness of plasters and textile reinforced mortars for strengthening clay masonry infill walls subjected to combined in-plane/out-of-plane actions. Mauerwerk 2015;19:334–54. https://doi.org/10.1002/dama.201500673.

[84] Furtado A, Rodrigues H, Arêde A, Varum H. Experimental characterization of the In-plane and Out-of-Plane behaviour of infill masonry walls. 1st Int Conf Struct Integr Influ (ICSI) 2015;114:862–9. https://doi.org/10.1016/j.proeng.2015.08.041.

[85] Furtado A, Rodrigues H, Arêde A, Varum H. Experimental evaluation of out-of-plane capacity of masonry infill walls. Eng Struct 2016;111:48–63. https://doi.org/10.1016/j.engstruct.2015.12.013.

[86] Singhal V, Rai DC. In-plane and out-of-plane behavior of confined masonry walls for various toothing and openings details and prediction of their strength and stiffness. Earthq Eng Struct Dyn 2016;45:2551–69. https://doi.org/10.1002/eqe.2783.

[87] Singhal V, Rai DC. Behavior of confined masonry walls with openings under In-Plane and Out-of-Plane loads. Earthq Spectra 2018;34:817–41. https://doi.org/10.1193/061416EQS097M.

[88] Sepasdar R. Experimental investigation on the Out-of-Plane behaviour of concrete masonry infilled RC frames. Halifax, Nova Scotia, Canada: MSc Thesis. Dalhousie University; 2017.

[89] Wang C. Experimental investigation on the Out-of-Plane behaviour of concrete masonry infilled frames. Halifax, Nova Scotia, Canada: MSc Thesis. Dalhousie University; 2017.

[90] Onat O, Correia AA, Lourenço PB, Koçak A. Assessment of the combined in-plane and out-of-plane behavior of brick infill walls within reinforced concrete frames under seismic loading. Earthq Eng Struct Dyn 2018;47:2821–39. https://doi.org/10.1002/eqe.3111.

[91] Ricci P, Di Domenico M, Verderame GM. Experimental assessment of the in-plane/out-of-plane interaction in unreinforced masonry infill walls. Eng Struct 2018;173:960–78. https://doi.org/10.1016/j.engstruct.2018.07.033.

[92] Ricci P, Di Domenico M, Verderame GM. Experimental investigation of the influence of slenderness ratio and of the in-plane/out-of-plane interaction on the out-of-plane strength of URM infill walls. Constr Build Mater 2018;191:507–22. https://doi.org/10.1016/j.conbuildmat.2018.10.011.

[93] Butenweg C, Marinković M, Salatić R. Experimental results of reinforced concrete frames with masonry infills under combined quasi-static in-plane and out-of-plane seismic loading. Bull Earthq Eng 2019;17:3397–422. https://doi.org/10.1007/s10518-019-00602-7.
[94] Marinković M, Butenweg C. Experimental testing of decoupled masonry infills with steel anchors for out-of-plane support under combined in-plane and out-of-plane seismic loading. Constr Build Mater 2022;318:126041. https://doi.org/10.1016/j.conbuildmat.2021.126041.
[95] De Risi MT, Di Domenico M, Ricci P, Verderame GM, Manfredi G. Experimental investigation on the influence of the aspect ratio on the in-plane/out-of-plane interaction for masonry infills in RC frames. Eng Struct 2019;189:523–40. https://doi.org/10.1016/j.engstruct.2019.03.111.
[96] Sagar SL, Singhal V, Rai DC. In-Plane and Out-of-Plane behavior of Masonry-Infilled RC frames strengthened with Fabric-Reinforced cementitious matrix. J Compos Constr 2019;23:1–14. https://doi.org/10.1061/(ASCE)CC.1943-5614.0000905.
[97] Akhoundi F, Vasconcelos G, Lourenco PB, Palha C. In-Plane and Out-of-Plane experimental characterization of RC masonry infilled frames. 6th Int Conf Mech Mater Des Port 2015:427–40.
[98] Akhoundi F, Vasconcelos G, Lourenço PB. Experimental Out-Of-Plane behavior of brick masonry infilled frames. Int J Archit Herit 2020;14:221–37. https://doi.org/10.1080/15583058.2018.1529207.
[99] da Porto F, Donà M, Verlato N, Guidi G. Experimental testing and numerical modeling of robust unreinforced and reinforced clay masonry infill walls, with and without openings. Front Built Environ 2020;6. https://doi.org/10.3389/fbuil.2020.591985.
[100] Santarsiero G, De Angelis A, Manfredi V, Santamato F, Masi A, Pecce M. Out-of-Plane ambient vibration tests of an infill wall in RC frame subjected to previous In-Plane damage. International Workshop on Civil Structural Health Monitoring (CSHM 2021), 156. Springer Science and Business Media Deutschland GmbH; 2021. p. 205–18. https://doi.org/10.1007/978-3-030-74258-4_14.
[101] Di Domenico M, De Risi MT, Ricci P, Verderame GM, Manfredi G. Empirical prediction of the in-plane/out-of-plane interaction effects in clay brick unreinforced masonry infill walls. Eng Struct 2021;227:111438. https://doi.org/10.1016/j.engstruct.2020.111438.
[102] Morandi P, Kurukulasuriya M, Milanesi RR, Bolognini D, Grottoli L, Dacarro F, et al. Dynamic shaking table out-of-plane tests on weak masonry infills with and without previous in-plane loading. J Build Eng 2025;100:111670. https://doi.org/10.1016/j.jobe.2024.111670.
[103] Henderson RC, Jones WD, Burdette EG, Porter ML. The effect of prior out-of-plane damage on the in-plane behavior of unreinforced masonry infilled frames. 4th DOE Natural Phenomena Hazards Mitigation Conference. Atlanta, Georgia, USA: Center for Natural Phenomena Engineering; 1993. p. 18.
[104] Palieraki V, Zeris C, Vintzileou E, Adami CE. In-plane and out-of-plane response of currently constructed masonry infills. Eng Struct 2018;177:103–16. https://doi.org/10.1016/j.engstruct.2018.09.047.
[105] Gkournelos PD, Triantafillou T. Integrated structural and energy retrofitting of masonry walls: the effect of In-Plane damage on the Out-Of-Plane response. 10th International Conference on FRP Composites in Civil Engineering (CICE). Istanbul, Turkey: Springer International Publishing; 2022. p. 1819–36. https://doi.org/10.1007/978-3-030-88166-5_157.
[106] Gkournelos PD, Triantafillou TC, Bournas DA. Integrated structural and energy retrofitting of masonry walls: effect of In-Plane damage on the Out-of-Plane response. J Compos Constr 2020;24:1–9. https://doi.org/10.1061/(ASCE)CC.1943-5614.0001066.
[107] Minotto M, Verlato N, Donà M, da Porto F. Strengthening of In-Plane and Out-of-Plane capacity of thin clay masonry infills using Textile- and Fiber-Reinforced mortar. J Compos Constr 2020;24. https://doi.org/10.1061/(ASCE)CC.1943-5614.0001067.
[108] Xie X, Qu Z, Fu H, Zhang L. Effect of prior in-plane damage on the out-of-plane behavior of masonry infill walls. Eng Struct 2021;226:111380. https://doi.org/10.1016/j.engstruct.2020.111380.
[109] Preti M, Migliorati L, Giuriani E. Experimental testing of engineered masonry infill walls for post-earthquake structural damage control. Bull Earthq Eng 2015;13:2029–49. https://doi.org/10.1007/s10518-014-9701-2.
[110] Milijaš A, Marinković M, Butenweg C, Klinkel S. Experimental investigation on the seismic performance of reinforced concrete frames with decoupled masonry infills: considering in-plane and out-of-plane load interaction effects. Bull Earthq Eng 2024;22:7489–546. https://doi.org/10.1007/s10518-024-02012-w.
[111] Korswagen PA, Longo M, Prosperi A, Rots JG, Terwel KC. Modelling of damage in historical masonry Façades subjected to a combination of ground settlement and vibrations. Struct Anal Hist Constr Cham Ger 2024:904–17. https://doi.org/10.1007/978-3-031-39603-8_73.
[112] Ghezelbash A, Beyer K, Dolatshahi KM, Yekrangnia M. Shake table test of a masonry building retrofitted with shotcrete. Eng Struct 2020;219:110912. https://doi.org/10.1016/j.engstruct.2020.110912.
[113] Wang X, Xiong L, Wang Z. Simplified model study of autoclaved aerated concrete masonry flexible connection infilled frames with basalt fiber grating strips. Buildings 2024;14:1033. https://doi.org/10.3390/buildings14041033.
[114] Morandi P, Hak S, Magenes G. Performance-based interpretation of in-plane cyclic tests on RC frames with strong masonry infills. Eng Struct 2018;156:503–21. https://doi.org/10.1016/j.engstruct.2017.11.058.
[115] Patel KP, Dubey RN. Effect of in-plane damage on the out-of-plane strength of masonry walls with openings. Structures 2024;65:106708. https://doi.org/10.1016/j.istruc.2024.106708.
[116] Asteris PG, Antoniou ST, Sophianopoulos DS, Chrysostomou CZ. Mathematical macromodeling of infilled frames: state of the art. J Struct Eng 2011;137:1508–17. https://doi.org/10.1061/(ASCE)ST.1943-541X.0000384.
[117] Pradhan B, Cavaleri L. IP-OOP interaction in URM infilled frame structures: a new macro-modelling proposal. Eng Struct 2020;224:111211. https://doi.org/10.1016/j.engstruct.2020.111211.
[118] Paulay T, Priestly MJN. Seismic design of reinforced concrete and masonry buildings. New York, USA: Wiley; 1992. https://doi.org/10.1002/9780470172841.
[119] Šakić B, Marinković M, Butenweg C, Klinkel S. Influence of slab deflection on the out-of-plane capacity of unreinforced masonry partition walls. Eng Struct 2023;276:115342. https://doi.org/10.1016/j.engstruct.2022.115342.
[120] Baek ER, Pohoryles DA, Bournas D. Seismic assessment of the in-plane/out-of-plane interaction of masonry infills in a two-storey RC building subjected to bi-directional shaking table tests. Earthq Eng Struct Dyn 2024;53:2230–51. https://doi.org/10.1002/eqe.4109.
[121] Gentile R, Angelucci G, Wu J, Di Benedetto M, Di Trapani F, Morandi P, et al. StateDepend Fragility via Exp Validated EnergyBased Approaches 2025:225–36. https://doi.org/10.1007/978-3-031-97129-7_18.
[122] Furtado A, Rodrigues H, Arêde A, Varum H. Modal identification of infill masonry walls with different characteristics. Eng Struct 2017;145:118–34. https://doi.org/10.1016/j.engstruct.2017.05.003.
[123] De Angelis A, Pecce MR. Out-of-plane structural identification of a masonry infill wall inside beam-column RC frames. Eng Struct 2018;173:546–58. https://doi.org/10.1016/j.engstruct.2018.06.072.
[124] Bolognini D, Dacarro F, Grottoli L, Milanesi RR, Morandi P. Development of a method based on audio waves for fast in-situ out-of-plane dynamic evaluations of the frequencies of masonry infills. Constr Build Mater 2024;452:138874. https://doi.org/10.1016/j.conbuildmat.2024.138874.
[125] Singhal V, Rai DC. In-plane and out-of-plane behavior of confined masonry walls for various toothing and openings details and prediction of their strength and stiffness. Earthq Eng Struct Dyn 2016;45:2551–69. https://doi.org/10.1002/eqe.2783.
[126] Furtado A, Rodrigues H, Arêde A, Varum H. Simplified macro-model for infill masonry walls considering the out-of-plane behaviour. Earthq Eng Struct Dyn 2016;45:507–24. https://doi.org/10.1002/eqe.2663.
[127] Mazza F. In-plane and out-of-plane nonlinear seismic response of masonry infills for hospitals retrofitted with hysteretic damped braces. Soil Dyn Earthq Eng 2021;148:106803. https://doi.org/10.1016/j.soildyn.2021.106803.
[128] Ricci P, Di Domenico M, Verderame GM. Out-of-plane seismic safety assessment of URM infills accounting for the in-plane/out-of-plane interaction in a nonlinear static framework. Eng Struct 2019;195:96–112. https://doi.org/10.1016/j.engstruct.2019.05.088.
[129] Ricci P, Di Domenico M, Verderame GM. Empirical-based infill model accounting for in-plane/out-of-plane interaction applied for the seismic assessment of EC8-designed RC frames. COMPDYN 2017 - Proceedings of the 6th International Conference on Computational Methods in Structural Dynamics and Earthquake Engineering, 2. National Technical University of Athens; 2017. p. 3380–97. https://doi.org/10.7712/120117.5652.18606.
[130] Morandi P., Hak S., Magenes G. Simplified Out-of-plane Resistance Verification for Slender Clay Masonry Infills in RC Frames. XV Convegno ANIDIS - "L'INGEGNERIA SISMICA IN ITALIA," Padova, Italy: 2013.
[131] Verlato N, Guidi G, da Porto F. Experimental testing and numerical modelling of infill masonry walls subjected to in-plane damage. 9th Int Mason Conf Guimaraes Port 2014.
[132] Al-Chaar G. Evaluating Strength and Stiffness of Unreinforced Masonry Infill Structures. Vicksburg, MS, USA: 2002.
[133] Rodrigues H, Varum H, Costa A. Simplified Macro-Model for infill masonry panels. J Earthq Eng 2010;14:390–416. https://doi.org/10.1080/13632460903086044.
[134] Shing PB, Cavaleri L, Di Trapani F. Prediction of the out-of-plane response of infilled frames under seismic loads by a new fiber-section macro-model. 16th International Brick and Block Masonry Conference, Padova, Italy. CRC Press; 2016. p. 1325–32. https://doi.org/10.1201/b21889-164.
[135] Furtado A, Rodrigues H, Arêde A, Varum H. Simplified macro-model for infill masonry walls considering the out-of-plane behaviour. Earthq Eng Struct Dyn 2016;45:507–24. https://doi.org/10.1002/eqe.2663.
[136] Cavaleri L, Di Trapani F. Cyclic response of masonry infilled RC frames: experimental results and simplified modeling. Soil Dyn Earthq Eng 2014;65:224–42. https://doi.org/10.1016/j.soildyn.2014.06.016.
[137] FEMA 273. Guidelines for the seismic rehabilitation of buildings. Washington, DC, USA: Federal Emergency Management Agency (FEMA); 1997.
[138] FEMA 356. Prestandard and commentary for the seismic rehabilitation of buildings. Reston, Virginia, USA: American Society of Civil Engineers (ASCE); 2000.
[139] ASCE 41-06. Seismic evaluation and retrofit of existing buildings. Reston, VA, USA: American Society of Civil Engineers (ASCE); 2006.
[140] ASCE 41-17. Seismic evaluation and retrofit of existing buildings. Reston, VA, USA: American Society of Civil Engineers (ASCE); 2017.
[141] New Zealand Society for Earthquake Engineering. The seismic assessment of existing buildings: part c - moment resisting frames with infill panels. Wellington, New Zealand: New Zealand Society for Earthquake Engineering (NZSEE); 2017.
[142] FEMA 306. Evaluation of Earthquake Damaged Concrete and Masonry Wall Buildings, 16. Redwood City, CA, USA: Applied Technology Council; 2000. https://doi.org/10.1193/1.1586111.

[143] Funari MF, Pulatsu B, Szabó S, Lourenço PB. A solution for the frictional resistance in macro-block limit analysis of non-periodic masonry. Structures 2022;43:847–59. https://doi.org/10.1016/j.istruc.2022.06.072.
[144] Ricci P, Di Domenico M, Verderame GM. Empirical-based out-of-plane URM infill wall model accounting for the interaction with in-plane demand. Earthq Eng Struct Dyn 2018;47:802–27. https://doi.org/10.1002/eqe.2992.
[145] Wilson R, Szabó S, Funari MF, Pulatsu B, Lourenço PB. A comparative computational investigation on the In-Plane behavior and capacity of Dry-Joint URM walls. Int J Archit Herit 2024;18:849–70. https://doi.org/10.1080/15583058.2023.2209776.
[146] Szabó S, Funari MF, Lourenço PB. Masonry patterns' influence on the damage assessment of URM walls: current and future trends. Dev Built Environ 2023;13:100119. https://doi.org/10.1016/j.dibe.2023.100119.